Chip

Review

PHOTONICS

DOI: 10.1016/j.chip.2023.100073

# Colloidal semiconductor nanocrystals for light emission and photonic integration

Huan Liu[1], Dabin Lin[1], Puning Wang[1], Tingchao He[2,*] & Rui Chen[1,*]

[1]*Department of Electrical and Electronic Engineering, Southern University of Science and Technology, Shenzhen 518055, China* [2]*Key Laboratory of Optoelectronic Devices and Systems of Ministry of Education and Guangdong Province, College of Physics and Optoelectronic Engineering, Shenzhen University, Shenzhen 518060, China*

*E-mails: tche@szu.edu.cn (Tingchao He), chenr@sustech.edu.cn (Rui Chen)

Cite as: Liu, H, Lin, D, Wang, P, He, T & Chen, R. Colloidal semiconductor nanocrystals for light emission and photonic integration. *Chip* **3**, 100073 (2024). https://doi.org/10.1016/j.chip.2023.100073

Received: 10 August 2023

Accepted: 15 October 2023

Published online: 20 October 2023

**Solution-processed colloidal semiconductor nanocrystals (NCs) have become attractive materials for the development of optoelectronic and photonic devices due to their inexpensive synthesis and excellent optical properties. Recently, CdSe NCs with different dimensions and structures have achieved significant progress in photonic integrated circuits (PICs), including light generation (laser), guiding (waveguide), modulation, and detection on a chip. This article summarizes the development of CdSe NCs–based lasers and discusses the challenges and opportunities for the application of CdSe NCs in PICs. Firstly, an overview of the optical properties of CdSe-based NCs with different dimensions is presented, with emphasis on the amplified stimulated emission and laser properties. Then, the nanophotonic devices and PICs based on CdSe NCs are introduced and discussed. Finally, the prospects for PICs are addressed.**

**Keywords:** CdSe nanocrystals, Amplified spontaneous emission, Waveguide, Laser, Photonic integrated circuits

## 1. INTRODUCTION

Nowadays, the explosive growth of global information has increased the demand for high-speed and low-cost information transmission technology and efficient central processing capacity[1]. Reducing the size of electronic chips and increasing the degree of integration are effective ways to achieve fast transmission efficiency. However, until now, integrated electronics that have reached the limit of Moore's Law are still unable to meet the requirements of high-speed information transmission[2,3]. In order to solve the bottleneck problem of semiconductor silicon chips, researches on photonic chips have attracted more and more attention due to its fast transmission speed, low power consumption, and large amount of information carried[4,5]. Generally, photonic integrated circuits (PICs) are composed of light sources, waveguides, optical processing components and photodetectors, which are integrated on wafers[3]. Among various types of PICs, Si-based PICs have witnessed rapid development due to their compatibility with mature complementary metal-oxide semiconductor (COMS), low cost, ultra-low waveguide loss and ease of fabrication[5,6]. However, due to the indirect bandgap of silicon, the lack of on-chip light sources remain a challenge for Si-based PICs[7]. Although GaAs can emit photons, it is not compatible with COMS[8,9]. Other II-VI and III-V semiconductor materials cannot simultaneously achieve light emission and process compatibility. Therefore, the development and application of advanced materials are critical for PICs.

Colloidal semiconductor nanocrystals (NCs) are a new class of nanomaterials with great potential in applications such as lasers and optoelectronic devices[10–14]. A distinct advantage of such NCs over conventional optical materials is that their emission can be tuned from the ultraviolet to the infrared wavelengths[11]. Optically tunable NCs can be synthesized by simple synthesis methods, and they exhibit good stability, solution processability, and high photoluminescence quantum yields (PLQY)[11]. Based on these excellent properties, Moungi G. Bawendi, Louis E. Brus, and Alexei I. Ekimov were awarded the Nobel Prize in Chemistry in 2023 for their discovery and development of colloidal NCs. At the same time, NCs are considered to be promising optical gain media for amplified spontaneous emission (ASE) and lasing[15,16]. In 2000, CdSe NCs ASE was first observed by Klimov et al[17]. In subsequent studies, many excellent CdSe-based NCs have been synthesized, including zero-dimensional (0D) core/shell quantum dots (QDs), alloy structures, giant NCs, one-dimensional (1D) nanorods (NRs), and quasi-two-dimensional (2D) nanoplatelets (NPLs)[18–22]. These CdSe-based NCs are excellent gain media and are combined with various microcavities such as whispering gallery modes (WGMs)[21,23], distributed feedback (DFB)[19,24], distributed Bragg reflector (DBR)[22], and Fabry-Pérot (FP) cavity[25], so as to form different types of lasers. At the same time, these wavelength-tunable CdSe-based NCs also exhibit a large refractive index[26], which is extremely beneficial for the construction of nanophotonic devices, such as waveguides, amplifiers and detectors. In addition, continuous-wave-pumped NC lasers and electrically pumped ASE have been realized recently[20,27–29], which have greatly stimulated the possibility for the application of CdSe NCs in PICs. However, the summary of these excellent CdSe NCs in ASE and lasing still remains insufficient. More importantly, the potential of CdSe

NCs as on-chip light sources needs to be further explored. Therefore, a prospective work is presented to demonstrate the important application prospects of CdSe NCs in PICs.

In this perspective, the optical properties of CdSe NCs with different morphologies are first presented. The optical gain, ASE and laser mechanisms, and optical losses are discussed. Then, the ASE mechanism and properties based on CdSe NCs are briefly summarized. Moreover, some methods to lower the gain threshold of CdSe based NCs and some advances in the optical gain of CdSe NCs are also proposed. Then, micro-/nano-lasers-based CdSe NCs, waveguides, photonic devices, and their on-chip integration are briefly summarized. Finally, the challenges and perspectives of NCs in PICs are presented.

## 2. THE OPTICAL PROPERTIES OF CdSe NCs

**2.1. Steady-state optical properties of CdSe NCs** Solution-processed semiconductor NCs have attracted considerable attention since their discovery due to their broadband absorption and tunable emission. So far, many colloidal NCs (including CdSe, ZnS, InP, $CuInS_2$, AgS) that exhibit good optical, electrical, and magnetic properties have been synthesized[35–40]. Among them, CdSe NCs have been extensively investigated due to their advantages such as high PLQY, good stability, facile synthesis methods and emission in the visible band[13,41,42]. In terms of morphology, CdSe NCs are divided into QDs, NRs and NPLs, as shown in the transmission electron microscope (TEM) image in Fig. 1a–c. Due to the quantum confinement effect, their absorption and emission can be tuned from the ultraviolet to the infrared regions, as shown in Fig. 1d–f. In addition, their different morphologies contribute to obvious differences in optical properties. For example, the full width at half maximum (FWHM) and Stokes shift of QDs, NRs, and NPLs gradually decrease, while the absorption cross-section gradually increases. The PLQY and optical stability of CdSe NCs will be difficult to be compared due to the different crystal quality and experimental conditions. In addition, the optical properties of CdSe NCs are affected by surface dangling bonds. In order to improve the optical properties and stability of CdSe NCs, these 0D QDs, 1D NRs, and 2D NPLs are usually coated with another semiconductor with a wider bandgap to passivate the surface defects, such as CdS, ZnS, ZnSe and CdTe[15,43–45]. These nano-heterojunctions (CdSe/CdS, CdSe/ZnS, CdSe/ZnSe core/shell etc.) exhibit superior optical properties compared to bare CdSe in terms of PLQY, fluorescence lifetime, absorption cross-section, stability, optical gain, etc.

**2.2. Optical gain, ASE, and laser mechanism** The optical gain of CdSe NCs is a crucial prerequisite for realizing NC PICs. Optical gain, which is also referred as population inversion, is related to the properties of the material itself. Optical gain is usually characterized with the adoption of a power-dependent pump-probe transient absorption (TA) technique[46]. Specifically, the optical density of the sample is $\Delta A + A_0$, where, $\Delta A$ denotes the absorbance change caused by light-induced absorption, and $A_0$ is the steady-state absorbance of the sample. NCs could produce optical gain when $\Delta A + A_0 < 0$ or the absolute value of $\Delta A/A_0$ is greater than 1[46]. At low power excitation, the TA spectrum of CdSe NCs only exhibits exciton bleaching. At this time, $\Delta A + A_0 > 0$, and no optical gain occurs, as shown in Fig. 2a. With the increase of power to its maximum value, an additional broadband negative peak is

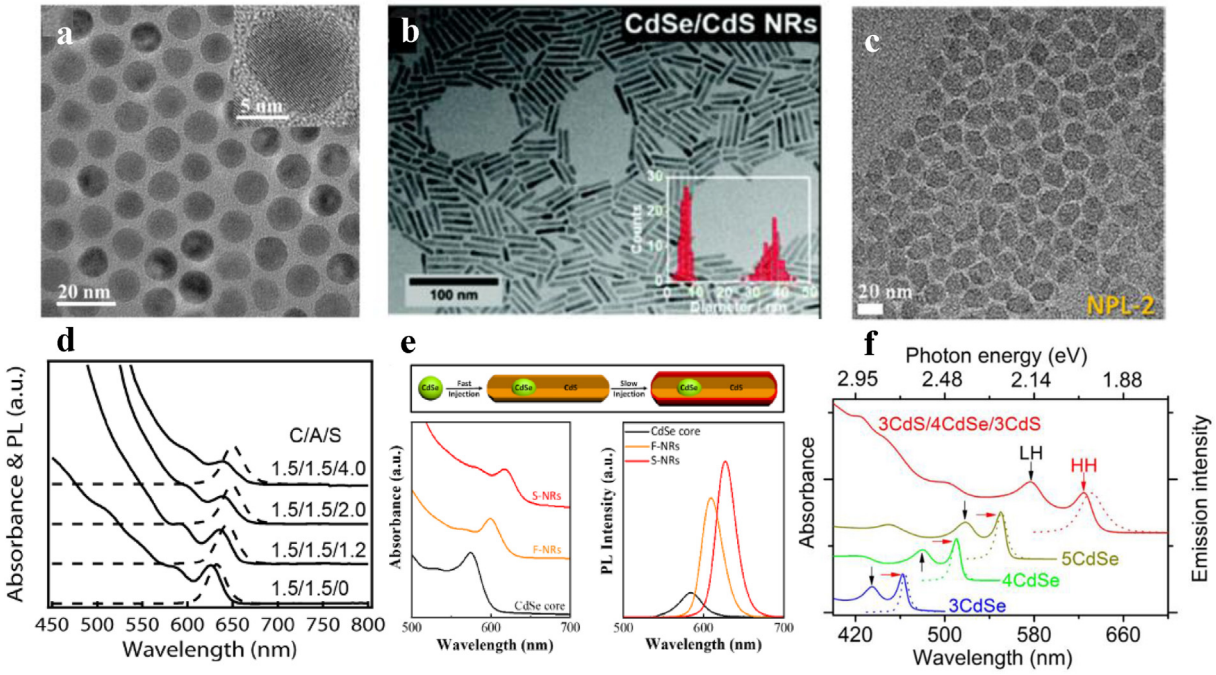


**Fig. 1 | a**, TEM images of the CdSe/CdS QDs. Reprinted with permission from ref.[19]. © 2017 American Chemistry Society. **b**, CdSe/CdS NRs. Reprinted with permission from ref.[30]. © 2020 The Royal Society of Chemistry. **c**, CdSe NPLs. Reprinted with permission from ref.[31]. © 2015 American Chemical Society. **d**, Absorption (solid lines) and emission (dashed lines) spectra of CdSe/$CdSe_xS_{1-x}$ QDs. Reprinted with permission from ref.[32]. © 2013 American Chemistry Society. **e**, Absorption and PL spectra of CdSe/CdS DIRs. Reprinted with permission from ref.[33]. © 2019 Optical Society of America. **f**, Absorption (solid lines) and emission (dashed lines) spectra of 3CdSe, 4CdSe, 5CdSe and 3CdS/4CdSe/3CdS NPLs. Reprinted with permission from ref.[34]. © 2015 American Chemistry Society. Abbreviatins: DIR: do-in-rod; NPL: nanoplatelet; PL: photolumiescence; QD: quantum dot; TEM: transmission electron microscope.

DOI: 10.1016/j.chip.2023.100073

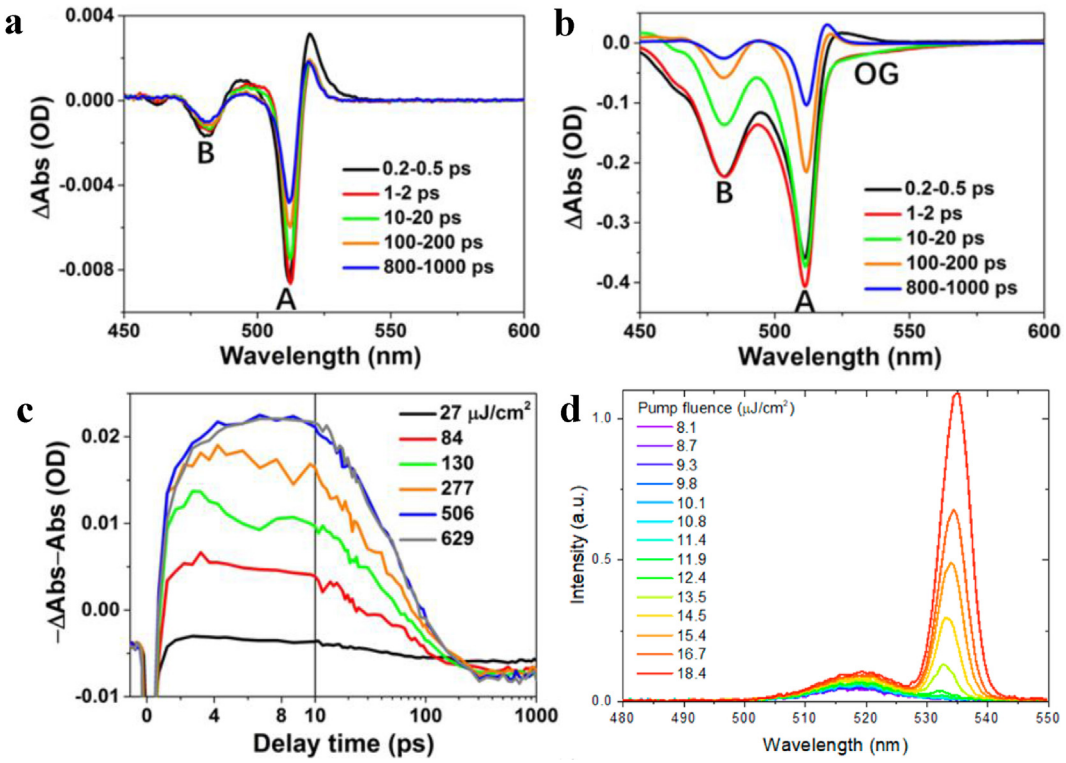


**Fig. 2 | TA spectra of CdSe NPLs at indicated delay times after 400 nm pump measured at a pump fluence of a,** 3 μJ/cm$^2$ and **b**, 629 μJ/cm$^2$**. c**, Optical gain kinetics at ~528 nm at different pump fluences of CdSe NPLs, reprinted with permission from ref.[46]. © 2018 The Royal Society of Chemistry. **d**, ASE spectra of a thin film of CdSe NPLs under increasing pump fluence. Reprinted with permission from ref.[47]. © 2018 American Chemical Society. Abbreviations: ASE: amplified spontaneous emission; NPL: nanoplatelet; TA: transient absorption.

exhibited on the low-energy side of the exciton-bleaching signal, as shown in Fig. 2b, which can be attributed to the optical gain of the NCs[20]. The optical gain threshold of the NCs can be obtained by extracting the signal of the broadband peak and then subtracting the steady-state absorbance, as shown in Fig. 2c. Different from optical gain, ASE is the amplification of spontaneously emitted photons by stimulated emission when propagating in the medium. The ASE of CdSe NCs is usually characterized by power-dependent fluorescence. However, it is worth noting that spontaneously emitted photons suffer optical losses when propagating through the medium. Therefore, at threshold power, the optical gain is greater than the optical loss, and an additional sharp peak appears on the spectrum, as shown in Fig. 2d [47]. The optical loss in NCs may be waveguide loss due to reabsorption. Recently, Ahn et al. found that the indium tin oxide (ITO) substrate would hinder the light amplification of NCs due to strong free-carrier absorption in the visible band when building a laser with an light-emitting diode (LED) structure[48–50]. Therefore, some materials can exhibit optical gain but fail to produce ASE once the optical loss is greater than the optical gain. Therefore, the gain capability, substrate selection, and reabsorption effect of the materials play a decisive role in the realization of ASE from NCs. Lasers are constructed by combining optical amplification of an optical gain medium with an optical resonant cavity. Therefore, the optical gain and optical loss of the laser depend on the ASE of the NCs. In addition to the induced optical loss of NCs, the substrate also affects the optical mode of NCs lasers. Recently, Ahn et al. found that the refractive index of the substrate will cause the NCs laser light field to be 'pulled', thereby increasing the waveguide loss[50]. In addition, the optical loss of the resonator also affects the threshold of the laser[51,52]. Compared with the ASE threshold, a high-quality resonator can lower the excitation threshold. Therefore, appropriate substrate and cavity design are also important for the NC lasers.

**2.3. Optical gain or ASE mechanism of CdSe QDs, NRs, and NPLs** An important requirement for the application of CdSe NCs in PICs is ASE since the information transfer of photonic chips depends on lasers with high monochromaticity and coherence. Over the past two decades, extensive breakthroughs and significant progress have been made in understanding the ASE properties of CdSe NCs[53,54]. In general, the realization of the ASE in CdSe QDs requires that the stimulated emission should overcome optical absorption[53,54]. The structural scheme of CdSe QDs ASE can be described by a two-level system. As shown in Fig. 3a, in the absence of optical pumping, two electrons with opposite spins are distributed in the ground state. Spontaneous emission is characterized by an electron being excited to the conduction band and then recombining with a hole to release a photon (Fig. 3b). This process does not produce stimulated emission due to the equal amount of spontaneous emission and optical absorption[53]. For CdSe QDs, due to the non-uniform degeneracy of the band-edge states, ASE is only possible when two electrons are excited into the conduction band to form a multi-exciton (Fig. 3c)[53]. Indeed, numerous experiments have been reported to demonstrate that the ASE of CdSe QDs is originated from multi-exciton recombination[53,54]. Moreover, the ASE is generally red-shifted relative to the spontaneous emission, which further confirms that the ASE of CdSe QDs is derived from multi-exciton recombination. Similar to CdSe QDs, the ASE mechanism of CdSe NRs and dot-in-rod (DIR) is also from biexciton[48,52,54]. However, the ASE mechanism of

DOI: 10.1016/j.chip.2023.100073

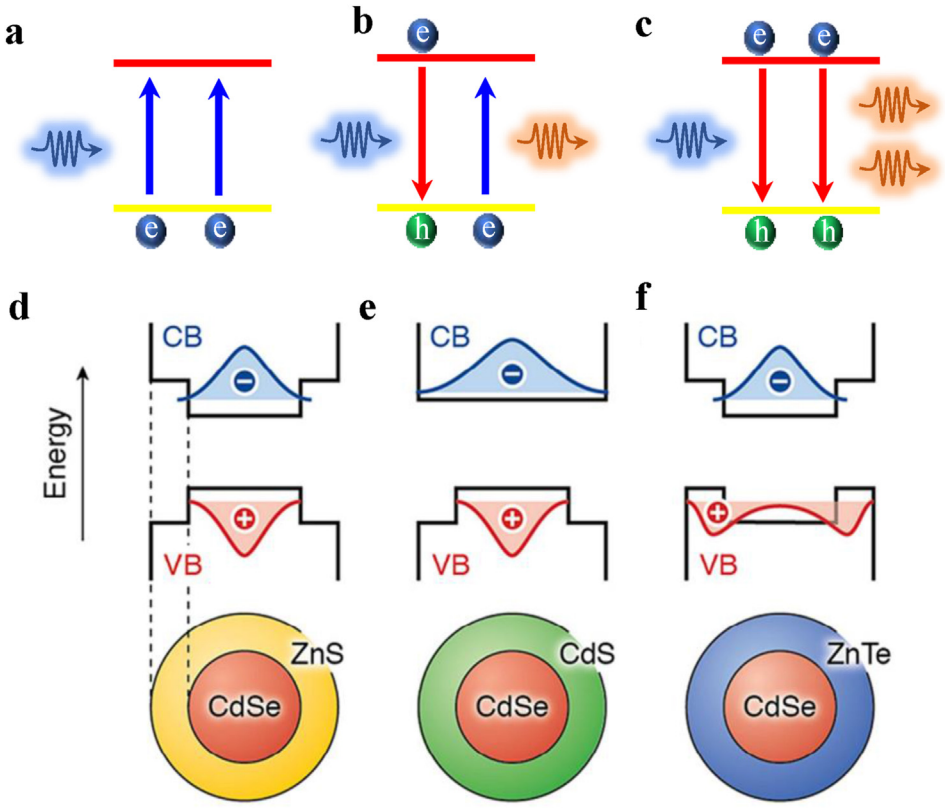


**Fig. 3 | Schematic illustration. a**, optical absorption. **b**, optical transparency. **c**, optical gain. Schematic illustration of energy band structure. **d**, Type I. **e**, Quasi II. **f**, Type II. Reprinted with permission from ref.[60]. © 2016 The Author(s).

CdSe NPLs is complex since it depends on the size and excitation density. Specifically, when the size of the CdSe NPLs is smaller than that of the Coulomb bound exciton, the optical gain of the CdSe NPLs is similar to that of the CdSe QDs, which is biexciton gain. However, when the lateral size of CdSe NPLs is larger than that of the Coulomb bound excitons, multiple excitons exist simultaneously in the same NPLs[46]. In this case, the maximum exciton number of CdSe NPLs depends on the size of NPLs rather than the state filling, which results in higher ASE threshold for larger-sized NPLs[31]. In addition to exciton states, the Coulomb-bound biexcitons may lead to optical gains of CdSe NPLs. This is ascribed to the fact that the biexciton binding energy of NPLs (30 to 40 meV) is greater than the room temperature thermal energy (25 meV), which allows the existence of biexcitons stably[27,55]. It is worth noting that since 2D NPLs could reduce dielectric shielding, the ASE mechanism of both large- and small-sized NPLs may be originated from Coulomb-bound biexcitons. In addition, when the NPLs are excited by high power density, the lattice heating generated by Auger decay and the increase in charge-carrier screening may dissociate the Coulomb-bound space, which may lead to stimulated emission from e-h plasma. In the study conducted by Tomar et al., it was found that CdSe NPLs exhibit Coulomb-bound biexciton gain when excited at low power[56]. With the increase of excitation power, an additional blue-shifted gain peak appears at the high-energy edge, which is the optical gain induced by e-h plasma. Although exciton-exciton scattering is also a common optical gain mechanism[57], this mechanism has not been observed in CdSe NCs. Although multiple mechanisms may act on the optical gain of CdSe NCs, the optical gain of the NCs regardless of the gain mechanism is hindered by the nonradiative Auger recombination (AR)[58]. Nonradiative AR can be explained by the fact that the energy of electron and hole recombination is transferred to a third particle (electron or hole), which is extremely disadvantageous for achieving ASE and lasing. In the last 20 years, many methods to suppress AR have been demonstrated, such as increasing the volume[19,54], changing the morphology of NCs[59], coating with wide bandgap materials, and smoothing the interface potential[32]. A more detailed discussion can be found in these reviews.

**2.4. ASE properties of CdSe QDs, NRs, and NPLs** The ASE of CdSe NCs (QDs) was first demonstrated by Klimov et al. in 2000[17]. This pioneering work revealed the underlying physical mechanism and conditions for the realization of NCs lasers and provided important guidance for the future exploration of NCs lasers. Following this work, CdSe NCs have been extensively investigated as a laser gain medium. To further lower the ASE threshold of CdSe NCs, wide bandgap shells (ZnS, CdS, CdTe, etc.) were deposited on the CdSe surface to suppress the AR caused by surface defects[32,61]. The absorption cross-section of the NCs was also simultaneously enhanced[54]. Due to the energy band misalignment between the CdSe core and the shell, the electron–hole wavefunction overlap is also an important factor for the optical gain of CdSe NCs. In general, the core/shell band alignment is classified into type I (Fig. 3d), quasi II (Fig. 3e), and type II (Fig. 3f). Compared with the type II and quasi II band alignments, the AR effect of the type I band alignment is the most intense since the electron–hole wave function is confined to the core. Although electrons and holes are separated the type II band alignment into different regions (core or shell), the reduced intensity of the optical oscillator strength makes it difficult to achieve optical gain. The CdSe NCs with quasi II band alignment are promising for optical devices because they not only delocalize the electron–hole

DOI: 10.1016/j.chip.2023.100073

wave function but also reduce defects[28]. For example, under the same conditions, the ASE threshold of type I CdSe/ZnS QDs (300 μJ/cm$^2$) under femtosecond laser pumping is an order of magnitude higher than that of quasi-II CdSe/CdS QDs (26 μJ/cm$^2$)[62]. In addition, the AR of CdSe NCs can be further suppressed by smoothing the core/shell interface with the adoption of the core/alloy/shell structure[32]. In a recent study performed by Klimov et al., electric pump gain was achieved for the first time adopting CdSe/Cd$_x$Zn$_{1-x}$Se/ZnSe$_{0.5}$S$_{0.5}$ core/alloy/shell structure with an Auger lifetime of 2.4 ns (Fig. 4a)[20]. For a more intuitive comparison, the optical gains of CdSe NCs with different types (morphology and band alignment) are summarized in Table 1, including ASE and laser threshold, emission wavelength and pump source. Obviously, for 0D CdSe QDs, the multi-shell alloy structure has the smallest ASE and laser threshold, which could be attributed to the passivating defects of multi-shell structure and the smoothing of the interface by the alloy structure.

Compared to 0D spherical QDs, CdSe NRs exhibit lower ASE thresholds due to the increase in absorption cross-section with increasing volume[69]. The charge carriers can move freely along the length of the NRs but are confined in the diameter direction[12,70]. The unique structure of NRs leads to different carrier relaxation and optical gain compared to QDs[59,70–72]. The lower ASE threshold of CdSe/ZnS NRs than that of QDs has been confirmed by Kazes et al. More importantly, the ASE of CdSe/ZnS NRs can be observed at room temperature, while that of QDs with the same diameter can only be observed at 50 K[73]. At the same time, it was also found that the ASE threshold of the CdSe/ZnS core/shell NRs remained constant below 120 K and increased with increasing temperature above 120 K due to Auger heating effect and phonon-assisted thermal relaxation. In addition to CdSe NRs, DIR nano-heterojunctions composed of CdSe QDs as cores and CdS NRs as shells have attracted more and more attention in recent years[69,74]. A lower gain threshold can be found in CdSe/CdS DIR than in CdSe/CdS QDs due to the larger volume of the former[69]. Importantly, the carriers transit from the core and shell states, respectively, leading to the observed two-color ASE in the core and shell of the CdSe/CdS DIR[66]. In addition, Iwan et al. found that the ASE threshold of CdSe/CdS DIR gradually decreased with increasing rod length[69]. At the same time, the ASE threshold of CdSe/CdS DIR is independent of temperature below 350 K, which is extremely important for on-chip lasers. Similarly, the ASE and laser characterization of different types of CdSe NRs are summarized in Table 1.

Compared with CdSe QDs and NRs, CdSe NPLs are the most promising in the application of ASE and lasers due to their extremely large absorption cross-section, giant oscillator strength, narrow emission band, and long Auger lifetime[31,47,76–78]. According to the unique layered structure, CdSe NPL heterojunctions can be divided into core/shell and core/crown structures[79,80]. In general, the CdSe core/shell NPL structure can achieve continuous regulation of the emission wavelength[68]. However, the CdSe core/shell NPLs structure also changes the emission FWHM and the quantum confinement effect in the vertical direction. For the CdSe core/crown NPL structure, the growth of the crown not only passivates the lateral defects of the NPLs, but also preserves the strong quantum confinement effect. Therefore, it is difficult to continuously tune the emission wavelength of the core/crown NPLs[34,81]. This difficulty has recently been addressed by Wu et al., which is beneficial for realizing continuous modulation of the on-chip laser peak[81]. For the same volume as CdSe QDs and NRs, NPLs exhibit lower ASE threshold, which may be related to the localized field and large absorption cross-section[54]. Taking advantage of the unique layered structure, CdSe NPLs can be stacked by special methods. As

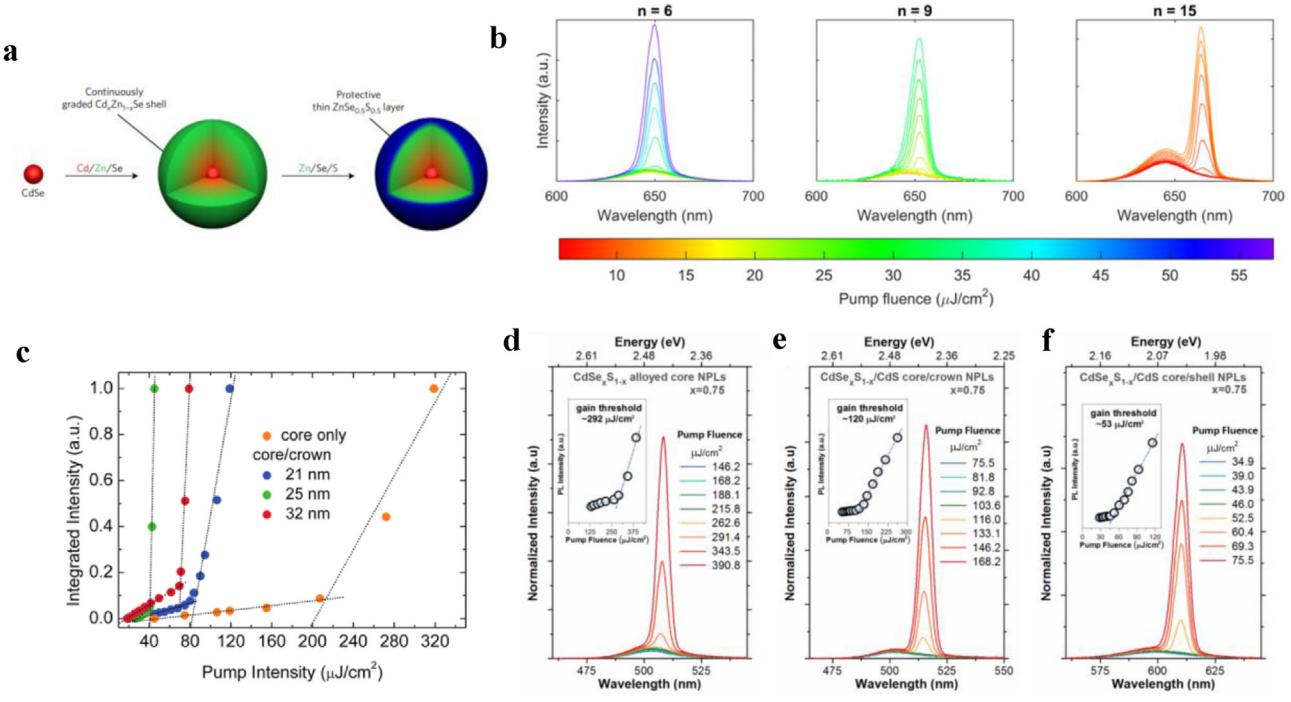


**Fig. 4 | a**, Schematic illustration of CdSe/Cd$_x$Zn$_{1-x}$Se/ZnSe$_{0.5}$S$_{0.5}$ QDs. Reprinted with permission from ref.[20]. © 2017 Macmillan Publishers Limited, part of Springer Nature. **b**, Emission spectra of CdSe/CdZnS core/shell NPLs films with different layers[75]. **c**, Integrated emission spectra of CdSe core and CdSe/CdS core/crown NPLs at different pump intensities[51]. **d**, Emission spectra of CdSe$_x$S$_{1-x}$ core. **e**, CdSe$_x$S$_{1-x}$/CdS core/crown. **f**, CdSe$_x$S$_{1-x}$/CdS core/shell NPLs[68]. Reprinted with permission from refs.[51,68,75]. © 2014, 2017, 2020 American Chemistry Society. Abbreviations: NPL: nanoplatelet; QD: quantum dot.

**Table 1 | Gain properties of CdSe nanocrystals with different morphologies.**

| Sample | ASE Peak (nm) | ASE thresholds | Laser thresholds | Cavity | Pump source | Ref. |
|---|---|---|---|---|---|---|
| CdSe QDs | 617 | N.A[a] | N.A | N.A | N.A | 17 |
| CdSe/CdS QDs | 642 | 108 μJ/cm$^2$ | 28 μJ/cm$^2$ | DFB | 400 nm (100 fs) | 19 |
| CdSe/CdZnSe/ZnSeS QDs | 620 | 3.3 μJ/cm$^2$ | N.A | N.A | 400 nm (100 fs) | 20 |
| CdSe/CdS/ZnO QDs | 632 | 28 μJ/cm$^2$ | 3.3 μJ/cm$^2$ | DBR | 400 nm (100 fs) | 63 |
| $Cd_{(1-x)}Zn_xSe_{(1-y)}S_y$/ZnS QDs | 532 | 80 μJ/cm$^2$ | 10.4 mJ/cm$^2$ | WGM | 400 nm (N.A ns) | 64 |
| CdSe/$Cd_xZn_{1-x}Se$/$ZnSe_{0.5}S_{0.5}$/ZnS QDs | 632 | 5.5 μJ/cm$^2$ | 5 μJ/cm$^2$ | DFB | 400 nm (130 fs) | 50 |
| CdSe/$Cd_xZn_{1-x}Se$/$ZnSe_{0.5}S_{0.5}$/ZnS QDs | ~645 | 13 A/cm$^2$ | N.A. | N.A. | Electricity (1.94 V) | 65 |
| CdSe/CdS QDs | 635 | N.A | 8.4 kW/cm$^2$ | PC-DFB | 442 nm (CW) | 28 |
| CdSe/ZnS NRs | 620 | 0.08 mJ | 3 mJ | WGM | 532 nm (5 ns) | 21 |
| CdSe/CdS DIRs | 600 | 1.5 mJ/cm$^2$ | 0.9 mJ/cm$^2$ | N.A | 800 nm (150 fs) | 52 |
| CdSe/CdS DIRs | 610 | N.A | 0.2 mJ/cm$^2$ | WGM | 400 nm (100 fs) | 66 |
| CdSe/CdS DIRs | 630 | 130 μJ/cm$^2$ | 10 μJ/cm$^2$ | N.A | 405 nm (70 fs) | 67 |
| CdSe NPLs | 532 | 45 μJ/cm$^2$ | N.A | N.A | 400 nm (120 fs) | 31 |
| CdSe NPLs | 532 | 5.5 mJ/cm$^2$ | N.A | N.A | 800 nm (120 fs) | 31 |
| CdSe NPLs | 532 | 6.5 W/cm$^2$ | 440 W/cm$^2$ | DBR | 444 nm (CW) | 27 |
| CdSe/CdS C/C NPLs | 534 | 41 μJ/cm$^2$ | N.A | N.A | 400 nm (120 fs) | 51 |
| CdSe/CdS C/C NPLs | 534 | 4.48 mJ/cm$^2$ | 2.49 mJ/cm$^2$ | DBR | 800 nm (120 fs) | 51 |
| CdSe/CdS C/S NPLs | 671 | 4.4 μJ/cm$^2$ | 1.1 μJ/cm$^2$ | DBR | 400 nm (100 fs) | 22 |
| CdSe/CdS/CdS C/C/S NPLs | 660 | 23 μJ/cm$^2$ | N.A | N.A | 400 nm (120 fs) | 45 |
| $CdSe_xS_{1-x}$ NPLs | 508 | 292 μJ/cm$^2$ | N.A | N.A | 400 nm (120 fs) | 68 |
| $CdSe_xS_{1-x}$/CdS C/C NPLs | 515 | 120 μJ/cm$^2$ | N.A | N.A | 400 nm (120 fs) | 68 |
| $CdSe_xS_{1-x}$/CdS C/S NPLs | 610 | 53 μJ/cm$^2$ | N.A | N.A | 400 nm (120 fs) | 68 |
| CdSe/CdS C/S NPLs | 635 | N.A | 1.2 mJ/cm$^2$ | N.A | 800 nm (150 fs) | 55 |
| CdSe/CdS C/S NPLs | 635 | N.A | 4.3 mJ/cm$^2$ | N.A | 1.3 μm (150 fs) | 55 |
| CdSe/CdS/$Cd_xZn_{1-x}S$ C/C/S NPLs | 637 | 17.2 μJ/cm$^2$ | 68 μJ/cm$^2$ | F–P | 400 nm (120 fs) | 25 |
| CdSe/CdSeTe C/C NPLs | 615 | 100 μJ/cm$^2$ | 950 μJ/cm$^2$ | Random | 530 nm (500 ps) | 43 |

[a] Not available. C/C, C/S, C/C/S NPLs represent core/crown, core/shell, and core/crown/shell, respectively. Abbreviations: ASE: amplified spontaneous emission; CW: continuous wave; DBR: distributed Bragg reflector; DFB: distributed feedback; DIR: dot-in-rod; NPL: nanoplatelet; NR: nanorod; PC-DFB: photonic crystal distributed feedback; QD: quantum dot; WGM: whispering gallery mode.

shown in Fig. 4b, the ASE threshold of CdSe NPLs can be gradually decreased with the increasing number of stacked layers[75]. Compared with bare CdSe NPLs, the ASE threshold can be lowered by growing a crown on the lateral surfaces to passivate the surface defects, as shown in Fig. 4c [51]. For the CdSe/$Cd_xZn_{1-x}S$ core/shell structure, the ASE peak position can be continuously regulated by adjusting the ratio of Zn and Cd in the shell. The minimum ASE threshold was found in the study by Volkan et al., when x was equal to 0.75[68]. For the $CdSe_xS_{1-x}$ core, $CdSe_xS_{1-x}$/CdS core/crown, and $CdSe_xS_{1-x}$/CdS core/shell NPLs, the $CdSe_xS_{1-x}$/CdS core/shell structure exhibits a low ASE threshold due to surface passivation and reduced AR rate (Fig. 4d–e). Unlike CdSe QDs and NRs, the ASE threshold of 2D NPLs tends to decrease with decreasing temperature due to the reduction of band-edge exciton degeneracy by exciton coherence region extension[82]. Exciton coherence extension does not occur in QDs and NRs[46,82]. Furthermore, Lian et al. found that the exciton coherence region of the CdSe NPLs decreases with increasing thickness of the NPLs[46,82]. Therefore, thin CdSe NPLs are potential candidates for the realization of on-chip lasers[83]. Similarly, the ASE and laser characterization of different types of CdSe NPLs are summarized in Table 1.

**2.5. Recent advances in ASE of CdSe NCs** As mentioned earlier, the ASE threshold of CdSe NCs could be determined by AR due to the degeneracy of the band-edge energy levels. How to suppress non-radiative AR and explore new optical gain methods has become a hot topic in the researches of optical gain in CdSe NCs. With the advancement of CdSe NCs synthesis methods and the design of advanced devices, some new ASE concepts have been demonstrated, such as single-exciton ASE, continuous-wave ASE, multi-photon and electric pump ASE. These advances provide important references for both lowering the ASE threshold of CdSe NCs and achieving the PICs.

*2.5.1. Single exciton ASE* Based on the optical gain model, the population inversion can only be achieved when the average exciton number of NCs is greater than N = 1 (the average number of excitons in NCs)[53,54,84]. However, if the optical gain can be achieved from single excitons instead of multi-excitons, the detrimental AR is not taken into consideration. In 2004, Ivanov et al. first developed and demonstrated single-exciton ASE from type II CdS/ZnSe[85]. The generation of single-exciton ASE is mainly ascribed to the formation of a local electric field after the generation of the excitons, resulting in an increase in the ground state absorption efficiency[85,86]. However, for conventional type I NCs, the ground-state absorption energy will be reduced due to exciton–exciton interactions. For type II NCs, there is a large exciton absorption energy due to the separation of the electron–hole wave function. Thus, single-exciton ASE has been demonstrated for the first time in type II CdS/ZnSe QDs[85]. As shown in Fig. 5a, two ASE peaks were observed in CdS/ZnSe QDs with increasing excitation power. Among them, the low-energy and high-energy ASE peaks are originated from single-exciton and biexciton gains, respectively. In 2012, the single-exciton ASE of red, green, and blue type I CdSe/ZnCdS core/shell QDs with aromatic ligands was confirmed by Dang et al.[87]. Recently, an optically doped sub-single-exciton ASE was demonstrated by Klimov et al.[88,89]. The schematic diagram of is shown in Fig. 5b. Specifically, the holes are trapped by a photo dopant (LiEt) after photoexcitation to generate an

DOI: 10.1016/j.chip.2023.100073

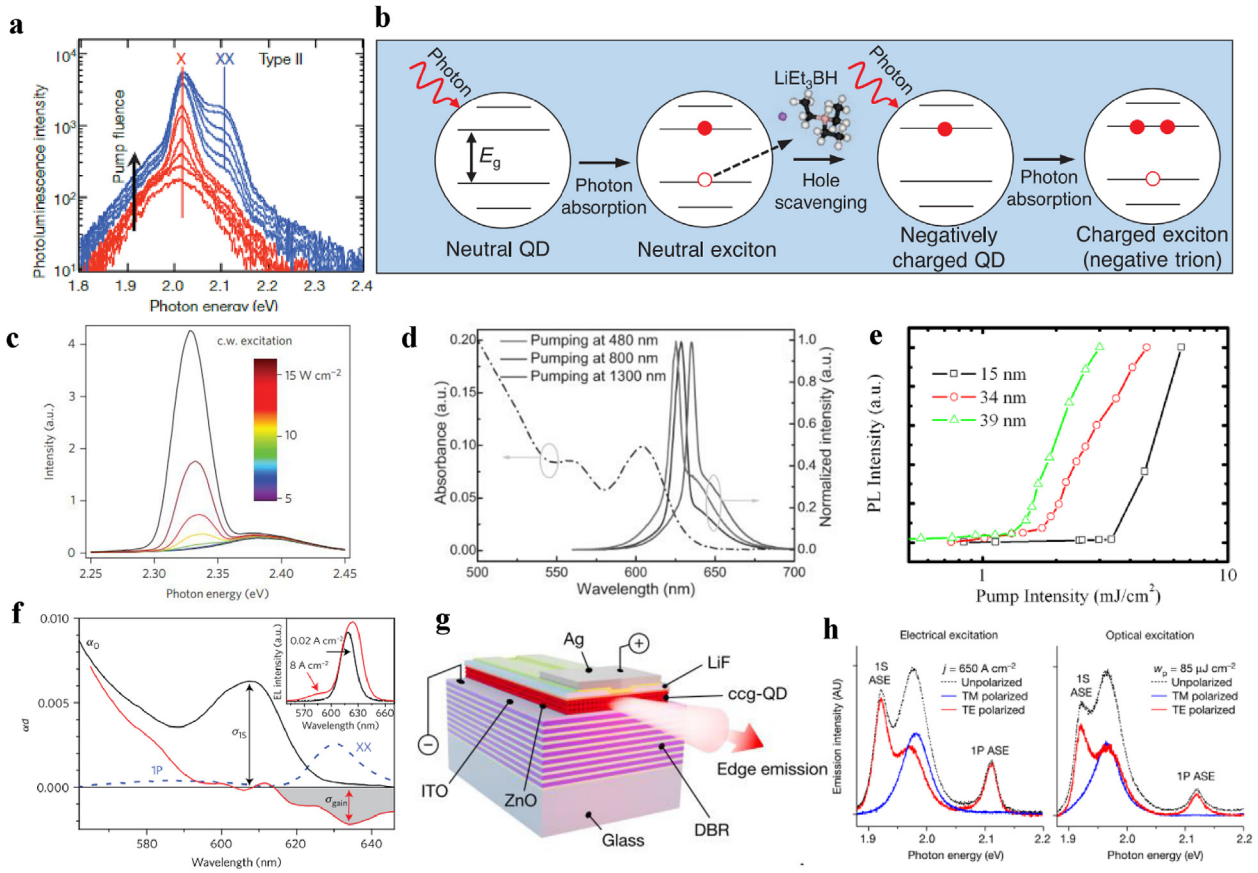


**Fig. 5 | a**, Single-exciton and biexciton ASE of type II CdS/ZnSe QDs. Reprinted with permission from ref.[86]. © 2007 Nature Publishing Group. **b**, Schematic diagram of charged exciton formation. Reprinted with permission from ref.[88]. © 2019 American Association for the Advancement of Science. **c**, ASE spectra of CdSe NPLs obtained under CW excitation. Reprinted with permission from ref.[27]. © 2014 Macmillan Publishers Limited. **d**, ASE spectra of CdSe/CdS/ZnS QDs under 400, 800, and 1300 nm pump. Reprinted with permission from ref.[90]. © 2014 WILEY-VCH Verlag GmbH & Co. KGaA, Weinheim. **e**, Integration intensity of CdSe/CdS DIR with different rod length emitted signal as a function of multi-photon pump power. Reprinted with permission from ref.[52]. © 2012 American Chemistry Society. **f**, Optical gain of CdSe/$Cd_xZn_{1-x}Se$/$ZnSe_{0.5}S_{0.5}$/ZnS QDs under electrical pumping. Reprinted with permission from ref.[20]. © 2017 Macmillan Publishers Limited, part of Springer Nature. **g**, Electrically pumped ASE structure in a Bragg reflective waveguide device. **h**, Polarization characteristics of edge-emitted light from the Bragg reflective waveguide device under electrical (left) and optical (right) excitation. Reprinted with permission from ref.[29]. © 2023 The Author(s). Abbreviations: ASE: amplified spontaneous emission; CW: continuous wave; DIR: dot-in-rod; NPL: nanoplatelet; QD: quantum dot.

exciton. Subsequently (about 30 min), when the composite of CdSe/CdZnSe NCs and photo dopant is excited for the second time, another electron is easily excited to the conduction band due to the disappearance of the local electric field[88,89]. Therefore, ASE is easily generated at sub-single exciton ($N$ = 0.3).

*2.5.2. Continuous-wave ASE* The realization of continuous wave (CW) pump ASE in NCs is highly desirable for the application of PICs. However, only a few CdSe NCs have been demonstrated for CW ASE. Thanks to the large absorption cross-section, large gain coefficient, and long Auger lifetime of CdSe NPLs, CW ASE was first confirmed by Grim et al. in 2014[27]. The ASE threshold of CdSe NPLs was confirmed to be 6 μJ/cm$^2$ under femtosecond-pulsed pumping (70 fs). Furthermore, the CW ASE threshold of CdSe NPLs was confirmed to be 6.5 W/cm$^2$ under 444 nm CW optical pumping (Fig. 5c). However, this result requires further confirmation due to the discrepancy between the thresholds of femtosecond pulse and CW pumping[53].

*2.5.3. Multi-photon pumped ASE* Multi-photon-pumped ASE is defined as multiple low-energy photons pumping CdSe NCs, followed by population inversion to generate optical gain[91]. In contrast to single-photon excitation, multi-photon-pumped ASE exhibits superliner absorption between the incident light, which results in deeper penetration depths and higher spatial resolution[92–94]. More importantly, the absorption losses caused by the waveguide material are unfavorable for PICs under single-photon pumping. This problem can be well-solved by multi-photon pumping. Taking advantage of the large multi-photon absorption cross-section and good photostability of CdSe NCs, multi-photon-pumped ASE have been found in CdSe QDs, NRs, and NPLs. In addition, for CdSe semiconductor heterojunctions, such as CdSe/CdS and CdSe/ZnS, the shell could increase the multi-photon absorption cross-section due to the antenna-like effect and the suppression of AR. In 2014, the ASE threshold of CdSe/CdS/ZnS QDs under two-photon pumping (Fig. 5d) was determined to be 8.2 mJ/cm$^2$ by Wang et al[90]. In addition, Xing et al. revealed the extremely low ASE threshold of

CdSe/CdS DIRs at 1.5 mJ/cm$^2$ under two-photon (800 nm) pumping, which is an order of magnitude smaller than that of the same type of QDs (Fig. 5e)[52]. The decrease in two-photon-pumped ASE threshold with increasing CdSe/CdS DIR length can be attributed to the increase of the two-photon absorption cross-section. Compared with QDs and NRs, a lower ASE threshold of 1.2 mJ/cm$^2$ for two-photon-pumped CdSe/CdS core/shell NPLs was demonstrated by Chan et al. At the same time, the ASE threshold of 4.3 mJ/cm$^2$ for three-photon-pumped CdSe/CdS core/shell NPLs was also confirmed by their group[55]. These multi-photons-pumped CdSe NCs ASE are not only of great importantance for life sciences but also hold important application prospects in the PICs.

*2.5.4. Electrically pumped ASE* Electrically pumped ASE based on semiconductor NCs have long been ideal devices due to their low substrate requirements, high scalability, and ease of on-chip photonics integration. Considerable efforts have been made to realize this exciting application. Recently, Klimov et al. demonstrated two-band (1S and 1P) electroluminescence with the adoption of continuously graded CdSe/Cd$_x$Zn$_{1-x}$Se/ZnSe$_{0.5}$S$_{0.5}$ QDs incorporated into a "current-focusing " LEDs structure. The population inversion of the band-edge 1S transition for electrically pumped CdSe/Cd$_x$Zn$_{1-x}$Se/ZnSe$_{0.5}$S$_{0.5}$ QDs was observed for the first time and was verified by adopting the current-modulated transient spectroscopy (Fig. 5f). Subsequently, their group reduced the thickness of the Cd$_x$Zn$_{1-x}$Se alloy layer and added a ZnS shell to suppress AR. Meanwhile, the electroluminescent structure is optimized by combining the DBR and the Ag mirror to form a lateral optical cavity, which improves the field confinement in the CdSe/Cd$_x$Zn$_{1-x}$Se/ZnSe$_{0.5}$S$_{0.5}$/ZnS QD gain medium and reduces the optical loss in the charge transport layer (Fig. 5g). Therefore, the room-temperature electrically pumped ASE of Cd-based colloidal QDs has been experimentally confirmed for the first time, as shown in Fig. 5h. This landmark result indicates that CdSe NCs with low substrate requirement, low gain threshold, and easy fabrication hold promising applications in future PICs.

## 3. APPLICATIONS

**3.1. CdSe NCs lasers with different resonator configurations** As the heart of PICs, lasers with high monochromaticity and coherence are essential. Transferring good, cheap lasers to tiny photonic chips is a goal currently pursued by the scientific community. Since CdSe NCs were demonstrated to exhibit ASE properties, many lasers based on CdSe NCs, including WGM, DFB, DBR, random lasers and photonic crystals have been demonstrated[19,21,22,65,95,96]. For example, a CdSe/CdS/ZnS QDs multimode WGM laser was constructed by Wang et al. by combining NCs with optical fibers (Fig. 6a)[97]. The lasing behavior is maintained at 312 K due to passivation by ZnS. Similarly, blue CdZnS/ZnS QDs WGM lasers have been confirmed by Sun et al. (Fig. 6b and c)[98]. CdSe NCs random laser is also a common laser, which is caused by the repeated scattering of light in the gain medium[65]. CdSe NCs random lasing usually consists of multiple peaks with different heights and positions. Although random lasers are efficient and inexpensive light

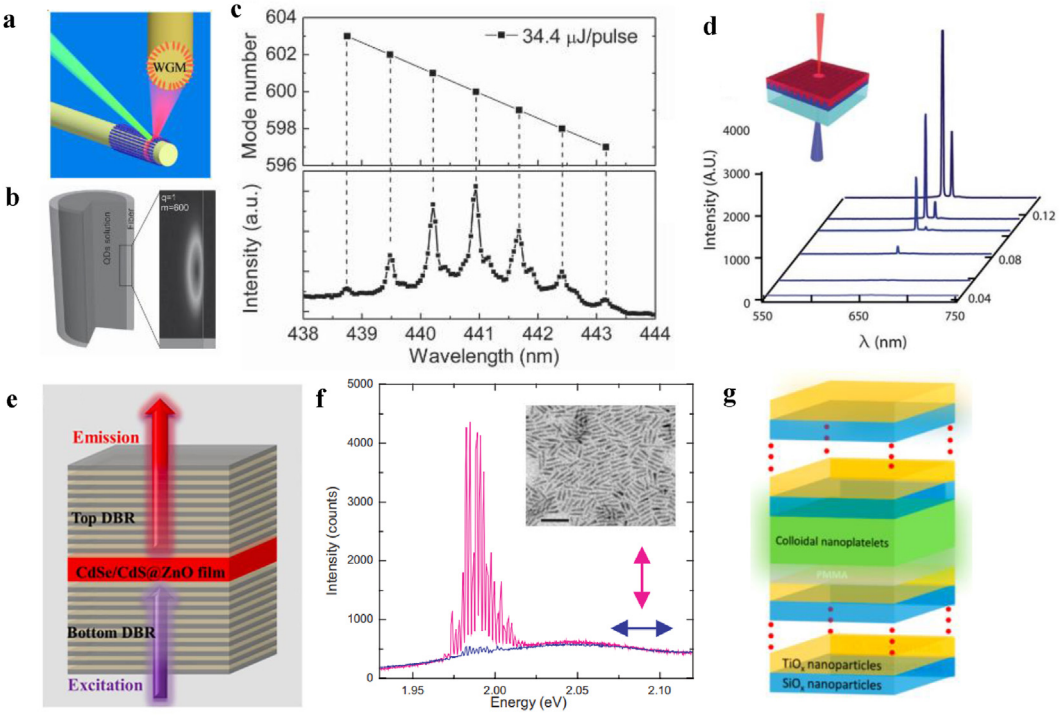


**Fig. 6 | a**, Schematic of WGM laser by coating QDs on fiber. Reprinted with permission from ref.[97]. © 2018 The Author(s). **b**, Electric field distribution in the radial direction for the WGM cavity. **c**, WGM lasing modes of CdZnS/ZnS QDs. Reprinted with permission from ref.[98]. © 2014 WILEY-VCH Verlag GmbH & Co. KGaA, Weinheim. **d**, Lasing emission spectra under different pump fluences. Reprinted with permission from ref.[99]. © 2011 The Royal Society of Chemistry. **e**, Schematic configuration of vertical cavity surface-emitting lasers using CdSe/CdS@ZnO QDs as gain medium. Reprinted with permission from ref.[63]. © 2021 Elsevier B.V. **f**, WGM lasing of CdSe/CdS NRs. Inset is TEM image of CdSe/CdS NRs. Reprinted with permission from ref.[21]. © 2022 WILEY-VCH Verlag GmbH. **g**, Schematic configuration of vertical cavity surface-emitting lasers using CdSe NPLs as gain materials. Reprinted with permission from ref.[51]. © 2014 American Chemistry Society. Abbreviations: NPL: nanoplatelet; NR: nanorod; QD: quantum dot; TEM: transmission electron microscope; WGM: whispering gallery mode.

sources, the poor quality and lack of directionality of the output light are detrimental to PICs. An efficient single mode laser can be constructed by coupling CdSe NCs and gratings to form DFB lasers. For example, single- and two-photon-pumped single-mode lasers have been realized by Signorini et al. by combining CdS/$Cd_{0.5}Zn_{0.5}S$/ZnS QDs with periodic gratings (Fig. 6d)[99]. Furthermore, ideal coherent single-mode lasing can be realized by confining CdSe NCs as laser gain materials to two highly reflective Bragg mirrors. As shown in Fig. 6e, CdSe/CdS–ZnO with FWHM 0.9-nm single-mode laser output is detected with the increase of pump intensity[63]. The same as QDs, CdSe NRs and NPLs, lasers with a lower lasing threshold can also be realized by combining gain materials with the aforementioned optical microcavities (Fig. 6f and g)[21,22,31,50,51,67,100,101]. Their laser characterization, cavity type, pump-light type, gain material, and other properties are summarized in Table 1. Combined with the advantages of easy preparation, low cost, solution treatment, and low substrate requirements, CdSe NCs can be used as potential candidates for on-chip light sources.

### 3.2. Recent advance in CdSe NCs lasing

*3.2.1. Single exciton lasers* As discussed in Section 2.3, single-exciton ASE, CW, and multi-photon-pumping ASE are novel and interesting optical phenomena. At the same time, single-exciton lasing, CW, and multi-photon-pumping lasing can be realized by incorporating CdSe NCs into resonant cavities. In 2012, the vertical cavity surface-emitting laser constructed by Dang et al. realized single-exciton ($N$ = 0.53) lasing by adopting CdSe/$Zn_{0.5}Cd_{0.5}S$ QDs and DBR as the gain medium and resonant cavity, respectively[87]. In 2019, the DFB single-mode laser was confirmed by Klimov et al. when pumped by a sub-single exciton (Fig. 7a)[88]. However, there exists a limitation that this photo dopant needs to be combined with Zn ions. Although there are relatively limited reports on NC single-exciton lasers, the profound advantages of NC lasers under single-exciton pumping are exciting since NCs with very fast Auger lifetimes can also achieve stimulated emission.

*3.2.2. CW lasing* Similarly, the construction of CW lasers is an important advance in the application of CdSe NCs to PICs. CW lasers were first realized by Grim et al. in 2014 by combining low-threshold CdSe NPLs with two Bragg mirrors. More recently, an extremely low-threshold (1 μW) CW laser was confirmed by Yang et al. by coupling CdSe/CdS core/shell NPLs to a photonic crystal nanobeam cavity[102]. However, real laser action and stimulated emission should be carefully distinguished. In 2017, Fan et al. developed a surface-selective growth shell on the core of CdSe QDs to separate band-edge degenerate states and thereby reduced the ASE threshold[28]. Importantly, the biaxially strained CdSe/CdS QDs are covered by a

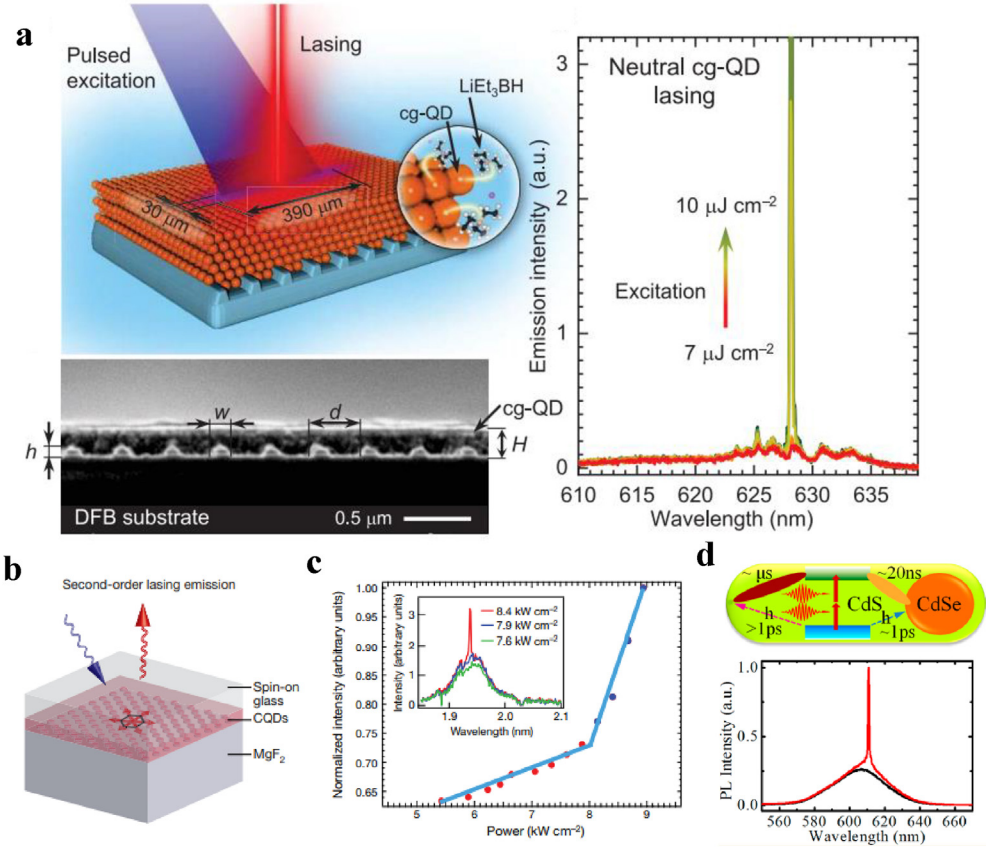


**Fig. 7 | a**, Schematics and SEM image of the CdSe/$Cd_xZn_{1-x}Se$/$ZnSe_{0.5}S_{0.5}$/ZnS QD DFB laser. Right: neutral-QD lasing spectra using a QD/DFB device. Reprinted with permission from ref.[88]. © 2019 American Association for the Advancement of Science. **b**, Schematics of CdSe/CdS QD PC-DFB laser. **c**, Integration of the emitted signal as a function of pump power. Inset is emission spectrum of above and below the lasering threshold. Reprinted with permission from ref.[28]. © 2017 Macmillan Publishers Limited, part of Springer Nature. **d**, Schematics and laser spectra of CdSe/CdS DIR under milti-photon pumping. Reprinted with permission from ref.[52]. © 2012 American Chemistry Society. Abbreviations: DFB: distributed feedback; NIR; PC-DFB: photonic crystal distributed feedback; QD: quantum dot.

2D photonic crystal (DFB) and exhibit lasing action in the range of 6.4 to 8.4 kW/cm$^2$ under CW pumping at 2.81 eV, as shown in Fig. 7b and c. This breakthrough development further clarifies the potential of CdSe NCs for application in PICs.

*3.2.3. Multi-photon pumped lasing* Although many organic dyes have achieved multi-photon-pumped lasing, semiconductor NCs can offer significant advantages for photonic chips in terms of their relatively large multi-photon absorption cross-section, high photostability, high refractive index, and low lasing threshold[103,104]. Compared with single-photon pumping, Wang et al. have confirmed for the first time that CdSe/CdS/ZnS QDs random laser exhibits weaker reabsorption effect under multi-photon pumping. In addition, ultra-low-threshold multi-photon-pumping laser was demonstrated by Li et al. in a cuvette containing CdSe/CdS core/shell NPLs solution[55]. Here, the CdSe/CdS core/shell NPLs and the cuvette act as the gain medium and the FP resonant cavity, respectively. The lasing thresholds of CdSe/CdS NPLs under pumping at two-photon (800 nm) and three-photon (1300 nm) pumping were characterized as 1.2 and 4.6 mJ/cm$^2$, respectively. Similarly, a vertical cavity surface-emitting laser was constructed by Volkan et al. by placing CdSe/CdS core/crown NPLs between two DBRs. The lasing threshold of CdSe/CdS core/crown NPLs was determined to be 2.49 mJ/cm$^2$ under two-photon pumping[51]. It is worth noting that, a lower two-photon-pumping lasing threshold (0.9 mJ/cm$^2$) was reported by Xing et al. in 2013 by coupling CdSe/CdS DIRs with a high-Q spherical optical cavity (Fig. 7d)[52]. Compared with QDs and NPLs, the lower two-photon lasing threshold of CdSe/CdS NRs in the current work may be related to the high Q factor spherical optical cavity.

**3.3. On-chip lasers based on CdSe NCs** As discussed in Section 2.2, considerable progress has been achieved by CdSe NCs in the field of ASE and lasers since the first demonstration of NCs optical gain. At the same time, CdSe NCs have also attracted special attention due to their potential to be used as light sources for PICs. According to the timeline, the on-chip laser formed by the integration of CdSe NCs and microcavities has undergone a transition from the uncontrollable stage to the controllable one[3]. At the early stage of on-chip laser-based NCs, Min et al. fabricated an on-chip WGM laser by covering CdSe/ZnS QDs on a ring-shaped fiber[105]. The pump pulse was efficiently coupled to the ring resonator through the tapered fiber (Fig. 8a), thus demonstrating the extremely low on-chip lasing threshold (9.9 fJ)[105]. However, complexity of the fibers for the output laser is not conducive to the realization of PICs. Therefore, the integration of microcavity and gain medium on the same substrate is beneficial for PICs. In the work of Wang et al., a WGM laser was confirmed by covering $Cd_{(1-x)}Zn_xSe_{(1-y)}S_y$/ZnS QDs to hemispherical resonator. The hemispherical resonator can be well mounted on the substrate to simplify the fabrication of the on-chip laser (Fig. 8b)[64]. In the construction of on-chip lasers, CdSe NCs were adopted as gain materials and resonators, which not only simplify the construction of on-chip light sources, but also reduce the cost of resonator construction. For example, CdSe/CdS QDs are drop-cast to form on-chip coffee rings as not only gain media, but also laser resonators. This coffee-ring effect can occur in CdSe QDs, NRs, NPLs, etc[66,108]. When the NC coffee ring is pumped, both sides can be used as an FP cavity to realize on-chip laser. In the work of Zavelani-Rossi et al., on-chip single mode lasers based on the coffee-ring effect of CdSe/CdS NIRs have also been demonstrated[66]. However, some disadvantages of coffee rings must be taken into

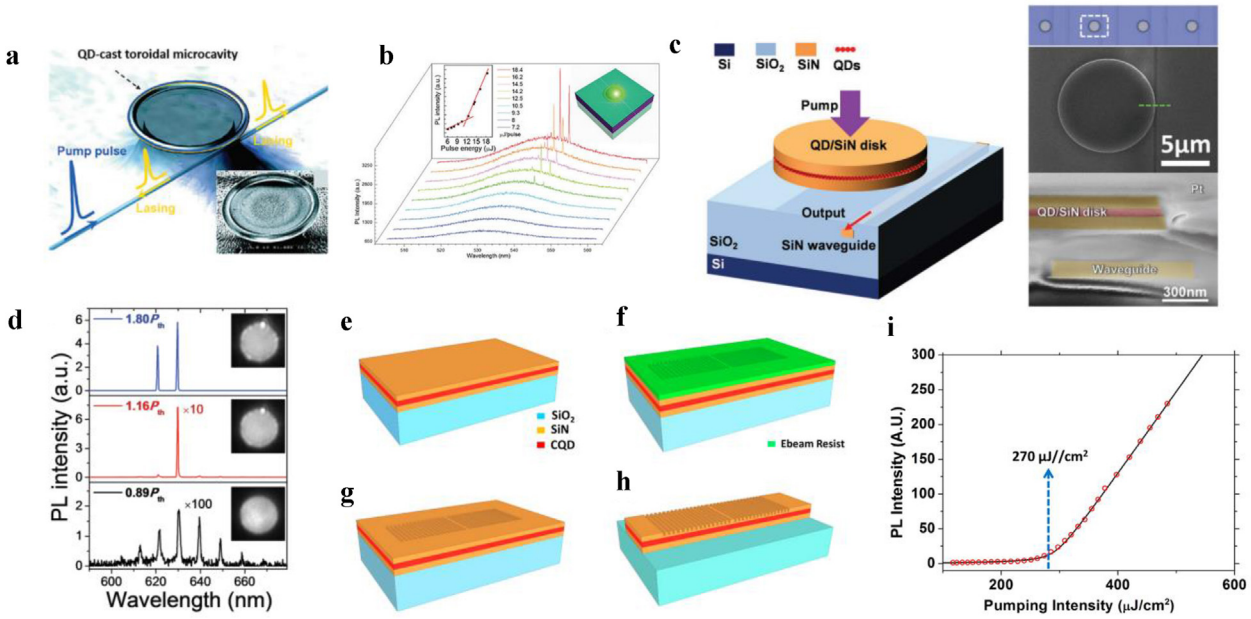


**Fig. 8 | a**, Schematic of a tapered fiber-coupled QDs laser. Reprinted with permission from ref.[105]. © 2006 American Institute of Physics. **b**, Laser spectra of QDs coated on self-assembled hemisphere with different excitation intensities. The insets are the integrated PL intensity with different pump fluences (left) and the schematic structure of the microlaser (right), respectively[64]. **c**, Schematic configuration of vertical coupling of SiN/QD/SiN disk and waveguide (left). SEM image of a fabricated device (right). **d**, Laser spectra of the SiN/QD/SiN disk under different pump fluences. Insets are corresponding PL images[106]. Reprinted with permission from refs.[64,106]. © 2015, 2017 WILEY-VCH Verlag GmbH & Co. KGaA, Weinheim. **e–h**, The process of resonator formation in the SiN/QDs/SiN plane waveguide. **i**, Integration of SiN/QDs/SiN laser-emitted signal as a function of the pump power. Reprinted with permission from ref.[107]. © 2017 American Chemistry Society. Abbreviations: PL: photoluminescence; QD: quantum dot; SEM: scanning electron microscopy.

DOI: 10.1016/j.chip.2023.100073

consideration, such as their uncontrollable size and position. Therefore, some high-precision control of the position, size, and laser peak position of on-chip NCs light sources have been realized in the recent years[26]. For example, Xie et al. designed a SiN/QDs/SiN (100/55/100 nm) planar sandwich-stack structure by e-beam lithography (EBL) etching method. A 5-μm-diameter micro-stage combined with CdSe/CdS QDs exhibited a low threshold fluence of 27 μJ/cm$^2$ WGM laser (Fig. 8c and d) under picosecond pulse pumping[106]. Subsequently, the transverse electric (TE)- and transverse magnetic (TM)-mode lasing of the QDs micro-stage was confirmed. In addition, single-mode lasers can also be observed by reducing the diameter of the microstage[106]. Similarly, DFB resonators in SiN/QDs/SiN plane waveguide were fabricated by their group with the adoption of the same etching method, as shown in Fig. 8e–h [107]. Single-mode lasing can be achieved by this SiN/QDs/SiN microstage at 270 μJ/cm$^2$ nanosecond-pulsed pumping (Fig. 8i). Such single-mode lasers show more potential in PICs due to fewer modes and higher optical purity. Moreover, these SiN/QDs/SiN sandwich structures with good compatibility with CMOS compatibility confirm that NCs are potential candidates for PICs[6]. However, some shortcomings still remain to be addressed. For example, the complex construction of these SiN/QDs/SiN and the fluorescence quenching caused by the high-temperature processing of NCs are not favorable for their future development. In addition, it should be noted that the current pump sources for on-chip lasers are all based on short-pulse lasers. More efforts are required to realize electrically pumped PICs so as to meet the current needs of high-speed information transmission.

**3.4. Integration of micro/nano lasers and waveguides** To further realize NCs PICs, on-chip integration of lasers and waveguides will be introduced. In general, on-chip integration of NCs-based active photonic devices and passive photonic devices based on other materials greatly increases the difficulty of fabricating PICs. Nevertheless, some noble progress in PICs based on NCs is worthy to be mentioned. For example, micro-stage multimode and single-mode lasers based on QDs have been demonstrated by Chen et al. adopting a simple and inexpensive approach[109]. The micro-stage (40 × 40 μm) was combined with a waveguide strip with a length of 150 μm and a width of 10 μm, as shown in Fig. 9a. When the pump pulse excites the micro-stage, the multimode laser spectra at $P_1$ and $P_2$ are collected as shown in Fig. 9b. This similar spectrum indicates that the laser propagates from the micro-stage $P_1$ to the waveguide $P_2$. Furthermore, no lasing was detected when the waveguide was pumped, confirming that the previous $P_2$ lasing is originated from the micro-stage. However, the position, size, and shape of the on-chip QDs laser and waveguide are uncontrollable. In addition, this waveguide composed of CdSe/ZnS QDs shows a large absorption loss because since the laser comes from the same NCs. In their other experiments, small-sized CdSe/ZnS QDs (green) as waveguides and large-sized CdSe/ZnSe/ZnS QDs as high-quality lasers were coupled on glass by pattern-assisted stacking to overcome absorption loss, as shown in Fig. 9c. Here, the lasing peak of CdSe/ZnSe/ZnS was found at 640 nm pumped by 532 nm ps pulses. As shown in Fig. 9d, the same lasing spectra obtained from A and B confirm that the micro-stage lasing from the red QDs can be coupled to the green waveguide. However, the disadvantage of this structure is that the laser and the waveguide are not on the same substrate, which results in an increase in the volume of the PICs and subsequent complex integration.

Position-, size-, and shape-controllable waveguides and lasers are confirmed by the Jeon's group by integrating lasers and SiN planar waveguides on a chip[111]. The schematic structure of these PICs is shown in Fig. 9e, where, $Si_3N_4$ and $SiO_2$ were used as the waveguide framework and substrate, respectively. Square lattices were constructed on 140-nm-thick $Si_3N_4$ by efficient EBL. CdSe/CdS/ZnS QDs were then selectively covered in the square lattice to form an on-chip laser. No etched $Si_3N_4$ acts as a waveguide due to the low absorption loss of

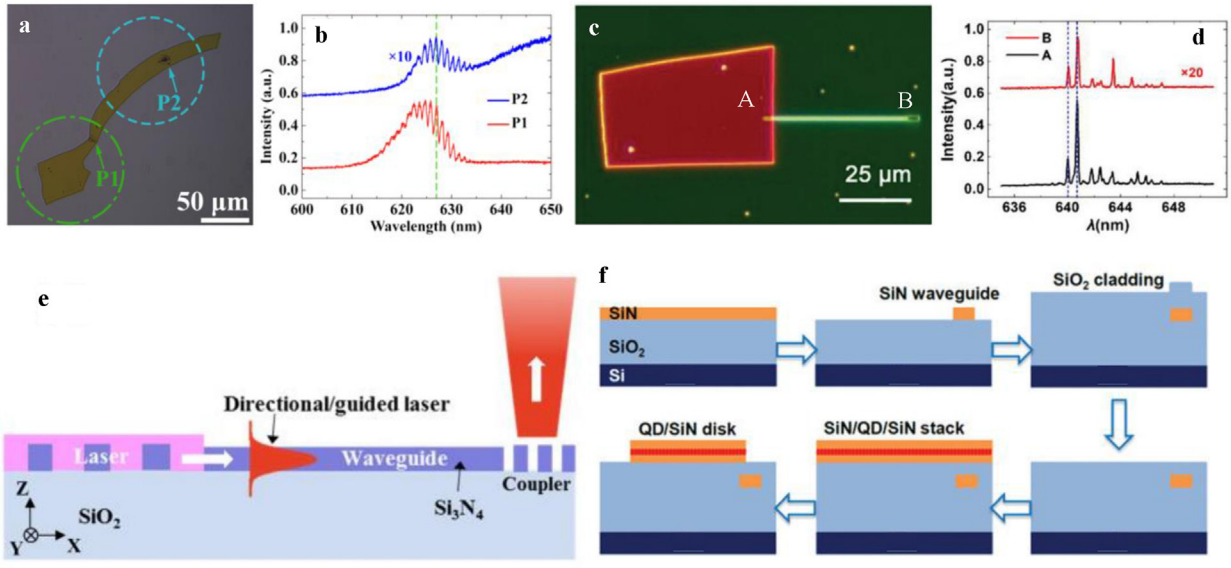


**Fig. 9 | a**, Bright-field optical image of integrating QDs microplate laser with waveguide. **b**, Laser emission spectra measured at $P_1$ (microplate laser) and $P_2$ (waveguide). Reprinted with permission from ref.[109]. © 2017 American Chemistry Society. **c**, Dark-field optical image of the integration of large CdSe/ZnSe/ZnS QDs high quality lasers with small CdSe/ZnS QDs (green) waveguides. **d**, Laser emission spectra measured at A (laser) and B (waveguide) in Fig. 9c.[110]. **e**, Schematic of integrating band-edge laser, waveguide, and output coupler on-chip[111]. Reprinted with permission from refs.[110,111]. © 2017, 2020 Optical Society of America. **f**, Schematic of the fabrication procedures for QDs micro-disk lasers integrated SiN waveguide. Reprinted with permission from ref.[106]. © 2017 WILEY-VCH Verlag GmbH & Co. KGaA, Weinheim. Abbreviation: QD: quantum dot.

DOI: 10.1016/j.chip.2023.100073

this structure in the visible to NIR. A grating coupler was placed at the other end of the waveguide. Therefore, the waveguide propagates the laser mode only in the vertical direction. When the QD-covered resonator was pumped, the single-mode laser was then coupled into the waveguide. Due to the presence of the grating coupler and the special thickness of the waveguide, the final laser was output in the vertical direction. This structure overcomes the formerly mentioned shortcomings that the position, size, and shape of the laser and the waveguide are not easy to be controled. More importantly, single-mode lasers were easily formed and efficiently coupled into the waveguides. However, the lack of lateral confinement of this planar waveguide may contribute to some crosstalk problems in future applications. Fortunately, this problem was solved in the same year by Dries Van's group[106]. As mentioned earlier, SiN/QDs/SiN sandwich structures have been placed on $SiO_2$ substrates to realize responsive WGM, and DFB lasers have been mentioned. In the current work, the on-chip laser and waveguide coupling were realized by this group. The construction and layout of these PICs is shown in Fig. 9f. In this structure, the structural parameters are carefully chosen to support TE and TM propagation. In addition to the coupling of dielectric waveguides and lasers, the coupling of plasmonic waveguides and lasers has also been demonstrated owing to the simple construction steps and low damage to the gain material. Specifically, Rong et al. adopted high-resolution dark-field optical imaging technology to integrate single or multiple microcavity lasers and silver nanowire waveguides on a chip, including tangential coupling, radial coupling and complex coupling[112]. As shown in Fig. 10a, the silver wire waveguide is placed in the tangential direction of the QDs micro-ring resonator. When the ring resonator is pumped, the emission spectra of the B and C ends of the silver wire are consistent with those of A, indicating that the laser is effectively coupled into the silver-wire waveguide (Fig. 10b). In addition, radial and tangential coupling of the microcavity laser to single or multiple silver-wire waveguides has also been demonstrated, as shown in the dark-field optical imaging diagram in Fig. 10c. Under picosecond laser pumping, the end of the silver-wire waveguide and the consistent spectrum of the microcavity laser indicate that the laser is coupled into multiple silver-wire waveguides. In addition, the coupling of multiple microcavity lasers to a silver-wire waveguide has also been demonstrated (Fig. 10d)[112]. This ease of operation is of great significance for realizing high-density assemblies of on-chip lasers, waveguides and functional devices.

**3.5. On-chip optical signal amplifier** Although the aforementioned studies show that the absorption and propagation losses of NC waveguides can be overcome by unique methods, potential losses still exist. Therefore, optical amplifiers are also crucial for NC PICs, especially for high-energy excitation of on-chip functional devices. The on-chip optical amplifier can directly amplify the optical signal without converting it to an electrical signal. Based on this situation, some designs of NC optical amplifiers have been proposed. The basic principle of the currently reported optical amplifier is that the optical signal generated by the on-chip laser propagates through the waveguide and is coupled to the optical amplifier to achieve signal amplification. In order to achieve optical signal amplification, high optical gain of NCs is a prerequisite. In 2017, Noriss et al. coupled NCs with surface plasmon

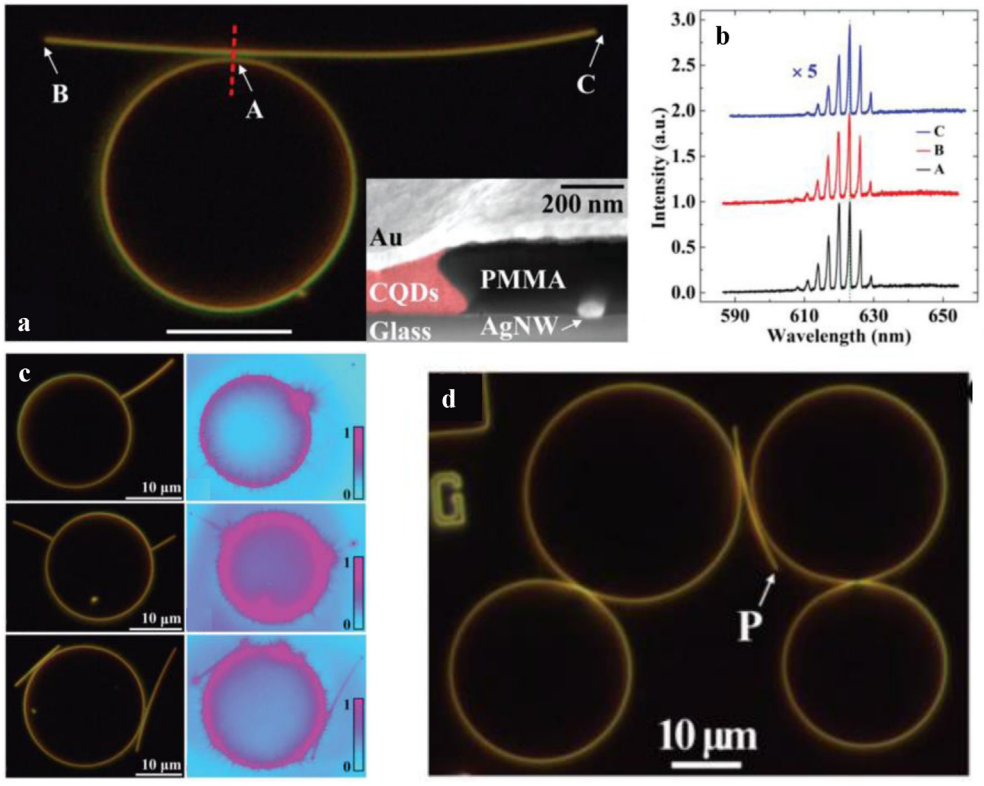


**Fig. 10 | a**, Dark-field optical image of the micro-ring resonator coupled with a tangential silver-nanowire waveguide. **b**, Laser emission spectra measured at A, B, and C in Fig. a. **c**, Dark-field optical image of coupling micro-ring resonator with single or multi tangential and radial silver-nanowire waveguides. On the right is the corresponding optical image under picosecond pulse pumping. **d**, Dark-field optical image of the coupling of multi micro-ring resonators with a tangential silver nanowire waveguide. Reprinted with permission from ref.[112]. © 2018 WILEY-VCH Verlag GmbH & Co. KGaA, Weinheim.

DOI: 10.1016/j.chip.2023.100073

systems to build on-chip lasers and optical amplifiers[113]. Specifically, two Ag reflective blocks with widths of 400 and 600 nm were extracted from the ultra-smooth silver surface to form a resonant cavity. Subsequently, a tapered waveguide was constructed by the template-stripping method, as shown in Fig. 11a. On-chip lasing was observed when CdSe/CdS/ZnS QDs covering the resonator were pumped by femtosecond pulses (Fig. 11b). After passing through the tapered waveguide, the on-chip laser is focused at the tip (Fig. 11c). Spectral characterization confirmed that the optical signal is extracted, propagated, and focused from the microcavity to the tip, as shown in Fig. 11d. However, the optical signal is not amplified due to propagation loss. When CdSe/CdS/ZnS QDs are simultaneously covered in the microcavity and the tapered waveguide, the on-chip laser can be amplified. The laser intensity of the waveguide with QDs covered is 1000-times higher than that of the waveguide without QDs, as shown in Fig. 11e and f. However, at low pump densities, the spontaneous emission noise is amplified by almost the same amount. In practical applications where pure signal amplification is required, the noise of these amplifications is undesirable. Recently, a noise-free optical amplifier has been proposed by Chen et al.[114]. Firstly, a micro-ring QD laser is constructed. Under picosecond pulse pumping, the on-chip laser is equally coupled to the left and right waveguides of different lengths ($L_L$ = 15 μm, $L_R$ = 40 μm) for signal transmission and optical signal amplification (Fig. 11g). Under small spot (17 μm) pumping, the laser intensity on the left is 1.3-times that of the right since part of the waveguide at the right end is not pumped (Fig. 11h). However, when the light spot size is increased to 80 μm, the light signal intensity on the right is 1.8-times that of the left (Fig. 11i). Importantly, the stimulated emission background signals on the left and right sides are the same sicne the laser signal is well coupled into the waveguide, while the stimulated emission is undirected. At the same time, this low-noise optical amplifier also prevents ASE generation along the NC waveguides.

**3.6. Integration of micro/nano lasers and functional devices** According to the aforementioned introduction, it can be known that PICs include light sources, waveguides, amplifiers, filters, detectors, and other devices. However, when these photonic devices are composed of different materials, the complexity, compatibility, and uncontrollability of photonic chips must be taken into consideration. Although many high-quality microcavity lasers and waveguides have been demonstrated and can be integrated on a chip as mentioned earlier, the integration of multifunctional devices, lasers, and waveguides remains a challenge. To solve the difficulty of integrating multiple functional devices on a chip, Rong et al. adopted the same QD material to construct multiple photonic devices on a chip by pattern-assisted stacking[114]. Firstly, a high-precision trench pattern is etched in the polymethyl methacrylate (PMMA) film with $MgF_2$ as the substrate. Subsequently, an appropriate QD solution is drop cast into the trenches to form on-chip lasers, waveguides, optical amplifiers, Y-splitters, and *Mach–Zehnder* interferometers, as shown in Fig. 12a–d. The same material is used to overcome the difficulty of building multiple photonic devices on a single chip. By combining the bottom-up and top-down approaches, the damage to the QDs could be negligible. However, absorption losses resulting from the use of the same material need to be considered. Although the current research on the integration of semiconductor microcavity lasers and functional devices is scarce, the continuous development of NC lasers and excellent photonic devices will promote the development of future photonic chips.

## 4. SUMMARY AND PROSPECTIVE

As electronic integrated circuits have reached the limits of Moore's Law, research on PICs has become one of the most rapidly developing fields. Despite the achievement of significant advances in the study of

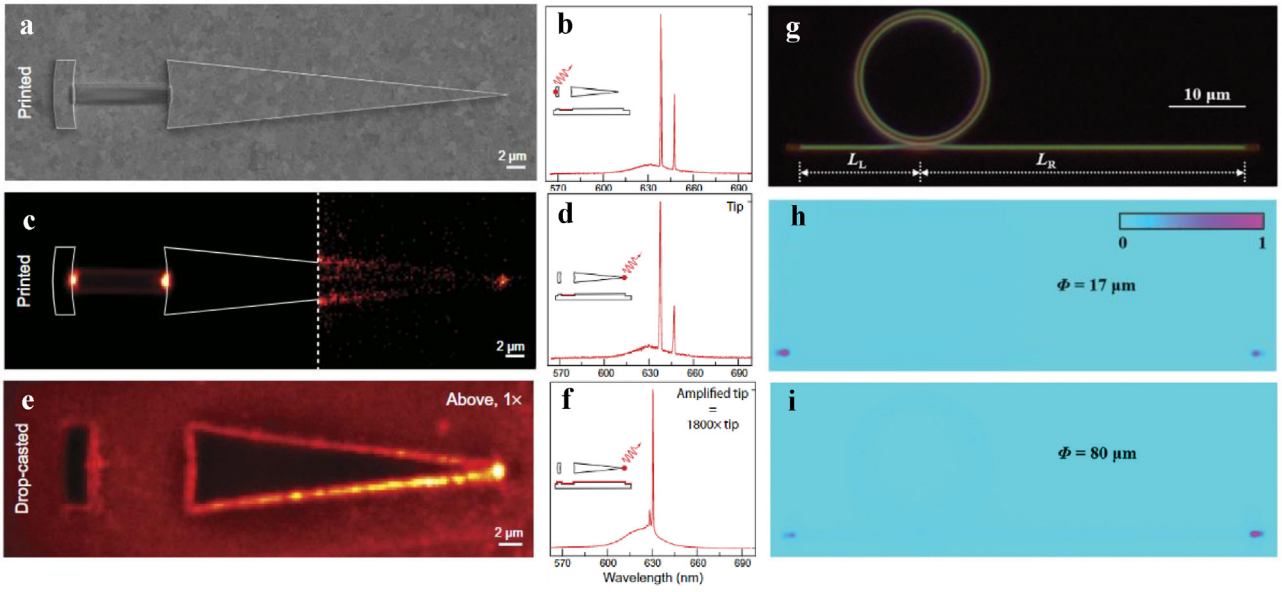


**Fig. 11 | a**, SEM image of the plasmonic resonator (left) and the tapered plasmonic waveguide (right). **b**, Laser spectra measured at the plasmonic resonator. **c**, Real-space image of the device in a. **d**, Laser spectra measured at the tip of the tapered plasmonic waveguide. **e**, Real-space image of the plasmonic resonator and tapered plasmonic waveguide coated with QDs. **f**, Laser spectra measured from the tip of waveguide coated with QDs. Reprinted with permission from ref.[113]. © 2017 The Authors. **g**, Dark-field image of optical amplifier with unequal waveguide length. Optical images of the amplifier under picosecond pulse pumping with a spot diameter of 17 (**h**) and 80 μm (**i**). Reprinted with permission from ref.[114]. © 2019 The Royal Society of Chemistry. Abbreviations: QD: quantum dot; SEM: scanning electron microscope.

ASE and laser properties and photonic devices based on CdSe NCs, PICs researches are still in the infant stage and full of challenges and opportunities. The combination of CdSe NCs and SiN platform has greatly accelerated the development of photonic chip. The unique photonic devices investigated by Chen et al. have also made significant contributions to the development of PICs[3,114]. However, there still exist pressing challenges in the synthesis of high-quality CdSe NCs, electrically pumped lasers, high-density integration of photonic devices, and environmentally friendly photonic chip. Based on some cutting-edge developments and ideas that have been presented recently, a personal view on the future development of laser manipulation and PICs is outlined as follows:

1) Electrically pumped lasers: an intriguing prospect of colloidal NCs is their application in electrically pumped lasers. Accordingly, semiconductor NCs are expected to exhibit excellent ASE and laser properties, which are critical in the PICs. However, at present, the pump source of NCs ASE and laser is still mainly short pulse. The main challenge remains AR, which leads to rapid deactivation of the semiconductor gain medium. How to suppress AR and thus reduce the laser threshold becomes the main difficulty for semiconductor NCs to be used in PICs. Some effective methods have been proposed for Auger suppression, such as surface passivation, alloy structure, and increasing the volume of NCs. Based on these methods, single-exciton-pumped laser[88], CW laser[28], electric pump optical gain[20], LED-like DFB structure have been demonstrated[50]. However, electric pump lasers are still not realized in NCs. Here, a personal view on the realization of electrically pumped lasers in NCs is outlined as follows: firstly, efforts should be devoted to high-quality NCs, such as NPLs with a slow AR. Secondly, finding suitable short-chain ligands to cover the surface of NCs may reduce the charge transport resistance. Thirdly, optimizing the device structure such as the charge transport layer for achieving more carrier balance injection. Fourthly, constructing high-quality resonators can facilitate further reduction in the threshold of lasers.
2) Integration of multifunctional photonic devices: the current semiconductor integrated circuit is based on Si technology, which involves the creation of multiple layers of interconnected electronic components on a silicon wafer. CdSe NCs can be synthesized in solution andsubsequently deposited onto various substrates for fabricating devices. Unfortunately, the Si substrate will absorb photons from the ultraviolet to near-infrared, which leads to additional absorption losses. As discussed in the main text, SiN cladding layers could reduce the influence of Si substrate; however, integration of photonic structure with electronics and another photonic element requires better strategies. Alternatively, a silicon-on-insulator wafer can be considered due to high refraction, which is good for effective light guiding and confinement. It is also good to act as a platform for integrating other electronic components such as transistors or waveguides[50,106]. Moreover, developing other gain materials such as colloidal PbS and HgTe semiconductor NCs to avoid the influence of Si substrate is another approach[115,116]. However, the PLQY of infrared QDs is much lower than that of CdSe NCs, and researches in the laser field still remain insufficient. More importantly, it is convenient for CdSe NCs to fabricate various photonic functional devices, including lasers, waveguides, detectors, modulators, etc. Therefore, photonic chips can be prepared by integrating different optoelectronic devices on the same substrate. However, researches on NC PICs are still in their infancy. Most reports have so far only achieved single-photonic devices. The integration of multiple-photonic devices still remains insufficient. The integration of full-function and high-density photonic devices is even more lacking. At the same time, the coupling efficiency between photonic devices and the absorption loss caused by the same NC material need to be taken into consideration. The integration of multifunctional photonic devices will mark a significant advance in PICs.
3) Environmentally friendly photonic chip: although the laser research of Cd and Pb NCs has become a hot topic due to their excellent optical properties, the construction of photon devices based on Cd- and Pb-containing NCs will inevitably lead to the problem of environmental pollution. Therefore, the emphasis of the future researches should also be laid upon the exploration of heavy-metal-free NCs, such as $CuInS_2$[38], InP/ZnSe/ZnS[39,117], and $ZnInS_2$[36],

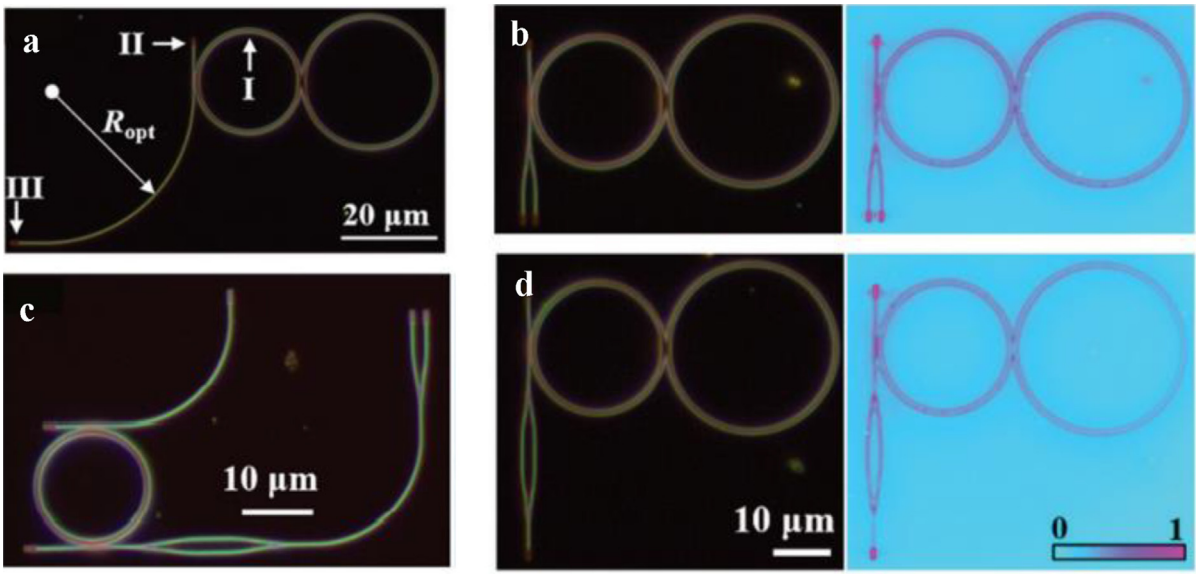


**Fig. 12 | a**, Dark-field optical image of the integrating resonator with bending waveguide. **b**, Optical images of the integrating resonator and the Y-splitter without (left) and with (right) pump pulse. **c**, Dark optical image of the integrating resonator, the MZ interferometer and the Y-splitter. **d**, Optical image and of the integrating resonator and the MZ interferometer without (left) and with (right) pump pulse. Reprinted with permission from ref.[114]. © 2019 The Royal Society of Chemistry. MZ: Mach–Zehnder.

ZnSe/ZnS[118]. Although the ASE and laser properties of these NCs are still immature, their relevant applications are expected to be realized through structural engineering and the design of suitable microcavity structures.

4) Others: just as the photonic devices mentioned earlier, the current NC photonic devices are all based on CdSe QDs, and the researches on NRs and NPLs with more excellent optical properties still remain insufficient. Therefore, more research efforts should be focused on the NRs and NPLs. In addition, considering that there are many studies on the nonlinear optical properties of CdSe NCs[37,55,119–121], more studies on their nonlinear optical pumping ASE and laser should be performed, with the aim of suppressing waveguide absorption losses and the construction of optical switches and modulators.

In summary, the foundation of semiconductor NCs lasers has been laid in the past two decades, and it is strongly expected that they could be used in photonic chips and explosively developed in the next two decades.

## REFERENCES


1. Margalit, N. et al. Perspective on the future of silicon photonics and electron-ics. *Appl. Phys. Lett.* **118**, 220501 (2021). https://doi.org/10.1063/5.0050117.
2. Xie, W. et al. Colloidal quantum dots enabling coherent light sources for integrated silicon-nitride photonics. *IEEE J. Sel. Top. Quantum Electron.* **23**, 8200913 (2017). https://doi.org/10.1109/JSTQE.2017.2737882.
3. Chen, J. & Rong, K. Nanophotonic devices and circuits based on colloidal quantum dots. *Mater. Chem. Front.* **5**, 4502–4537 (2021). https://doi.org/10.1039/D0QM01118E.
4. Chen, Y. et al. Integrated quantum nanophotonics with solution-processed materials. *Adv. Quantum Technol.* **5**, 2100078 (2022). https://doi.org/10.1002/qute.202100078.
5. Roeloffzen, C. G. H. et al. Silicon nitride microwave photonic circuits. *Opt. Express* **21**, 22937–22961 (2013). https://doi.org/10.1364/OE.21.022937.
6. Xiang, C., Jin, W. & Bowers, J. E. Silicon nitride passive and active photonic integrated circuits: trends and prospects. *Photonics Res.* **10**, A82–A96 (2022). https://doi.org/10.1364/PRJ.452936.
7. Vannahme, C., Klinkhammer, S., Lemmer, U. & Mappes, T. Plastic lab-on-a-chip for fluorescence excitation with integrated organic semiconductor lasers. *Opt. Express* **19**, 8179–8186 (2011). https://doi.org/10.1364/OE.19.008179.
8. Kang, Y. et al. Controlled synthesis of pure-phase GaAs nanowires through shear tension. *ACS Photonics* **8**, 2889–2897 (2021). https://doi.org/10.1021/acsphotonics.1c01196.
9. Li, H., Chen, Y., Wei, Z. & Chen, R. Optical property and lasing of GaAs-based nanowires. *Sci. China Mater.* **63**, 1364–1381 (2020). https://doi.org/10.1007/s40843-020-1288-6.
10. Diroll, B. T. et al. 2D II-VI semiconductor nanoplatelets: from material synthesis to optoelectronic integration. *Chem. Rev.* **123**, 3543–3624 (2023). https://doi.org/10.1021/acs.chemrev.2c00436.
11. Pietryga, J. M. et al. Spectroscopic and device aspects of nanocrystal quantum dots. *Chem. Rev.* **116**, 10513–10622 (2016). https://doi.org/10.1021/acs.chemrev.6b00169.
12. Wu, K. & Lian, T. Quantum confined colloidal nanorod heterostructures for solar-to-fuel conversion. *Chem. Soc. Rev.* **45**, 3781–3810 (2016). https://doi.org/10.1039/c5cs00472a.
13. Altintas, Y. et al. Giant alloyed hot injection shells enable ultralow optical gain threshold in colloidal quantum wells. *ACS Nano* **13**, 10662–10670 (2019). https://doi.org/10.1021/acsnano.9b04967.
14. Kim, W. D. et al. Pushing the efficiency envelope for semiconductor nanocrystal-based electroluminescence devices using anisotropic nanocrystals. *Chem. Mater.* **31**, 3066–3082 (2019). https://doi.org/10.1021/acs.chemmater.8b05366.
15. Gao, Y. et al. Photophysical properties of water-soluble CdTe/CdSe/ZnS core/shell/shell nanocrystals emitting at 820 nm. *J. Phys. Chem. C* **124**, 7994–7999 (2020). https://doi.org/10.1021/acs.jpcc.0c01027.
16. Yu, P. et al. Highly efficient green InP-based quantum dot light-emitting diodes regulated by inner alloyed shell component. *Light: Sci. Appl.* **11**, 162 (2022). https://doi.org/10.1038/s41377-022-00855-z.
17. Klimov, V. I. et al. Optical gain and stimulated emission in nanocrystal quantum dots. *Science* **290**, 314–317 (2000). https://doi.org/10.1126/science.290.5490.314.
18. Wang, S. et al. Low-threshold amplified spontaneous emission in blue quantum dots enabled by effectively suppressing auger recombination. *Adv. Opt. Mater.* **9**, 2100068 (2021). https://doi.org/10.1002/adom.202100068.
19. Zhang, L. et al. Single-mode lasing from "giant" CdSe/CdS core-shell quantum dots in distributed feedback structures. *ACS Appl. Mater. Interfaces* **9**, 13293–13303 (2017). https://doi.org/10.1021/acsami.7b01669.
20. Lim, J., Park, Y.-S. & Klimov, V. I. Optical gain in colloidal quantum dots achieved with direct-current electrical pumping. *Nat. Mater.* **17**, 42–49 (2018). https://doi.org/10.1038/nmat5011.
21. Kazes, M., Lewis, D. Y., Ebenstein, Y., Mokari, T. & Banin, U. Lasing from semiconductor quantum rods in a cylindrical microcavity. *Adv. Mater.* **14**, 317–321 (2002). https://doi.org/10.1002/1521-4095(20020219)14:4<317::AID-ADMA317>3.0.CO;2-U.
22. Zhang, L. et al. Low-threshold amplified spontaneous emission and lasing from thick-shell CdSe/CdS core/shell nanoplatelets enabled by high-temperature growth. *Adv. Opt. Mater.* **8**, 1901615 (2020). https://doi.org/10.1002/adom.201901615.
23. Wu, Y. et al. A new generation of liquid lasers from engineered semiconductor nanocrystals with giant optical gain. *Laser Photonics Rev.* **17**, 2200703 (2023). https://doi.org/10.1002/lpor.202200703.
24. Zhang, Q. et al. Low-threshold single-mode microlasers from green CdSe/CdSeS core/alloyed-crown nanoplatelets. *ACS Photonics* **10**, 1397–1404 (2023). https://doi.org/10.1021/acsphotonics.3c00018.
25. Maskoun, J. et al. Optical microfluidic waveguides and solution lasers of colloidal semiconductor quantum wells. *Adv. Mater.* **33**, 2007131 (2021). https://doi.org/10.1002/adma.202007131.
26. Lin, C. H. et al. Large-scale robust quantum dot microdisk lasers with controlled high quality cavity modes. *Adv. Opt. Mater.* **5**, 1700011 (2017). https://doi.org/10.1002/adom.201700011.
27. Grim, J. Q. et al. Continuous-wave biexciton lasing at room temperature using solution-processed quantum wells. *Nat. Nanotechnol.* **9**, 891–895 (2014). https://doi.org/10.1038/nnano.2014.213.
28. Fan, F. et al. Continuous-wave lasing in colloidal quantum dot solids enabled by facet-selective epitaxy. *Nature* **544**, 75–79 (2017). https://doi.org/10.1038/nature21424.
29. Ahn, N. et al. Electrically driven amplified spontaneous emission from colloidal quantum dots. *Nature* **617**, 79–85 (2023). https://doi.org/10.1038/s41586-023-05855-6.
30. Lübkemann, F. et al. Reversible cation exchange on macroscopic CdSe/CdS and CdS nanorod based gel networks. *Nanoscale* **12**, 5038–5047 (2020). https://doi.org/10.1039/c9nr09875e.
31. Olutas, M. et al. Lateral size-dependent spontaneous and stimulated emission properties in colloidal CdSe nanoplatelets. *ACS Nano* **9**, 5041–5050 (2015). https://doi.org/10.1021/acsnano.5b01927.
32. Bae, W. K. et al. Controlled alloying of the core-shell interface in CdSe/CdS quantum dots for suppression of auger recombination. *ACS Nano* **7**, 3411–3419 (2013). https://doi.org/10.1021/nn4002825.
33. Zhang, Y. et al. High-efficiency CdSe/CdS nanorod-based red light-emitting diodes. *Opt. Express* **27**, 7935–7944 (2019). https://doi.org/10.1364/OE.27.007935.
34. She, C. et al. Red, yellow, green, and blue amplified spontaneous emission and lasing using colloidal CdSe nanoplatelets. *ACS Nano* **9**, 9475–9485 (2015). https://doi.org/10.1021/acsnano.5b02509.
35. Liu, H., Shang, G., Ren, C., Gao, Y. & He, T. Photophysical properties of Mn-doped InP/ZnS nanocrystals. *J. Phys. Chem. C* **125**, 21748–21753 (2021). https://doi.org/10.1021/acs.jpcc.1c06858.
36. Gao, Y. et al. Efficient multiphoton absorption of near-infrared emitting Cu-doped ZnInS/ZnS nanocrystals. *J. Phys. D: Appl. Phys.* **53**, 255103 (2020). https://doi.org/10.1088/1361-6463/ab7e65.
37. He, T. et al. Water-soluble chiral CdSe/CdS dot/rod nanocrystals for two-photon fluorescence lifetime imaging and photodynamic therapy. *Nanoscale* **11**, 15245–15252 (2019). https://doi.org/10.1039/c9nr04508b.
38. Li, L. et al. Efficient synthesis of highly luminescent copper indium sulfide-based core/shell nanocrystals with surprisingly long-lived emission. *J. Am. Chem. Soc.* **133**, 1176–1179 (2011). https://doi.org/10.1021/ja108261h.
39. Liu, H. et al. InP semiconductor nanocrystals: synthesis, optical properties, and applications. *Adv. Opt. Mater.* **11**, 2300425 (2023). https://doi.org/10.1002/adom.202300425.
40. Carey, G. H. et al. Colloidal quantum dot solar cells. *Chem. Rev.* **115**, 12732–12763 (2015). https://doi.org/10.1021/acs.chemrev.5b00063.
41. Hao, J. et al. Ligand-induced chirality in asymmetric CdSe/CdS nanostructures: a close look at chiral tadpoles. *ACS Nano* **14**, 10346–10358 (2020). https://doi.org/10.1021/acsnano.0c03909.

42. Bertrand, G. H. V., Polovitsyn, A., Christodoulou, S., Khan, A. H. & Moreels, I. Shape control of zincblende CdSe nanoplatelets. *Chem. Commun.* **52**, 11975−11978 (2016). https://doi.org/10.1039/c6cc05705e.
43. Gao, Y. et al. Low-threshold lasing from colloidal CdSe/CdSeTe core/alloyed-crown type-II heteronanoplatelets. *Nanoscale* **10**, 9466−9475 (2018). https://doi.org/10.1039/c8nr01838c.
44. Gao, Y. et al. Linear and nonlinear photophysical properties of ZnSe/CdS/ZnS core/shell/shell type II nanocrystals. *Photonics Res.* **8**, 1416−1421 (2020). https://doi.org/10.1364/prj.387099.
45. Kelestemur, Y. et al. Platelet-in-box colloidal quantum wells: CdSe/CdS@CdS core/crown@shell heteronanoplatelets. *Adv. Funct. Mater.* **26**, 3570−3579 (2016). https://doi.org/10.1002/adfm.201600588.
46. Li, Q. & Lian, T. A model for optical gain in colloidal nanoplatelets. *Chem. Sci.* **9**, 728−734 (2018). https://doi.org/10.1039/c7sc04294a.
47. Guzelturk, B., Pelton, M., Olutas, M. & Demir, H. V. Giant modal gain coefficients in colloidal II-VI nanoplatelets. *Nano Lett.* **19**, 277−282 (2019). https://doi.org/10.1021/acs.nanolett.8b03891.
48. Ahn, N., Livache, C., Pinchetti, V. & Klimov, V. I. Colloidal semiconductor nanocrystal lasers and laser diodes. *Chem. Rev.* **123**, 8251−8296 (2023). https://doi.org/10.1021/acs.chemrev.2c00865.
49. Ahn, N. et al. Optically excited lasing in a cavity-based, high-current density quantum dot electroluminescent device. *Adv. Mater.* **35**, 2206613 (2023). https://doi.org/10.1002/adma.202206613.
50. Roh, J., Park, Y.-S., Lim, J. & Klimov, V. I. Optically pumped colloidal-quantum-dot lasing in LED-like devices with an integrated optical cavity. *Nat. Commun.* **11**, 271 (2020). https://doi.org/10.1038/s41467-019-14014-3.
51. Guzelturk, B., Kelestemur, Y., Olutas, M., Delikanli, S. & Demir, H. V. Amplified spontaneous emission and lasing in colloidal nanoplatelets. *ACS Nano* **8**, 6599−6605 (2014). https://doi.org/10.1021/nn5022296.
52. Xing, G. et al. Ultralow-threshold two-photon pumped amplified spontaneous emission and lasing from seeded CdSe/CdS nanorod heterostructures. *ACS Nano* **6**, 10835−10844 (2012). https://doi.org/10.1021/nn304200a.
53. Wang, Y. & Sun, H. Advances and prospects of lasers developed from colloidal semiconductor nanostructures. *Prog. Quantum Electron.* **60**, 1−29 (2018). https://doi.org/10.1016/j.pquantelec.2018.05.002.
54. Park, Y.-S., Roh, J., Diroll, B. T., Schaller, R. D. & Klimov, V. I. Colloidal quantum dot lasers. *Nat. Rev. Mater.* **6**, 382−401 (2021). https://doi.org/10.1038/s41578-020-00274-9.
55. Li, M. et al. Ultralow-threshold multiphoton-pumped lasing from colloidal nanoplatelets in solution. *Nat. Commun.* **6**, 8513 (2015). https://doi.org/10.1038/ncomms9513.
56. Tomar, R. et al. Charge carrier cooling bottleneck opens up nonexcitonic gain mechanisms in colloidal CdSe quantum wells. *J. Phys. Chem. C* **123**, 9640−9650 (2019). https://doi.org/10.1021/acs.jpcc.9b02085.
57. Shi, Y. et al. Laser-induced secondary crystallization of $CsPbBr_3$ perovskite film for robust and low threshold amplified spontaneous emission. *Adv. Funct. Mater.* **32**, 2207206 (2022). https://doi.org/10.1002/adfm.202207206.
58. Makarov, N. S. et al. Spectral and dynamical properties of single excitons, biexcitons, and trions in cesium-lead-halide perovskite quantum dots. *Nano Lett.* **16**, 2349−2362 (2016). https://doi.org/10.1021/acs.nanolett.5b05077.
59. Chhantyal, P. et al. Low threshold room temperature amplified spontaneous emission in 0D, 1D and 2D quantum confined systems. *Sci. Rep.* **8**, 3962 (2018). https://doi.org/10.1038/s41598-018-22287-9.
60. Rabouw, F. T. & de Mello Donega, C. Excited-state dynamics in colloidal semiconductor nanocrystals. *Top. Curr. Chem.* **374**, 58 (2016). https://doi.org/10.1007/s41061-016-0060-0.
61. Reiss, P., Protiere, M. & Li, L. Core/Shell semiconductor nanocrystals. *Small* **5**, 154−168 (2009). https://doi.org/10.1002/smll.200800841.
62. García-Santamaría, F. et al. Suppressed auger recombination in "giant" nanocrystals boosts optical gain performance. *Nano Lett.* **9**, 3482−3488 (2009). https://doi.org/10.1021/nl901681d.
63. Zhang, L. et al. High-performance CdSe/CdS@ZnO quantum dots enabled by ZnO sol as surface ligands: a novel strategy for improved optical properties and stability. *Chem. Eng. J.* **428**, 131159 (2022). https://doi.org/10.1016/j.cej.2021.131159.
64. Wang, Y., Yang, S., Yang, H. & Sun, H. Quaternary alloy quantum dots: toward low-threshold stimulated emission and all-solution-processed lasers in the green region. *Adv. Opt. Mater.* **3**, 652−657 (2015). https://doi.org/10.1002/adom.201400528.
65. Park, Y.-S., Bae, W. K., Baker, T., Lim, J. & Klimov, V. I. Effect of auger recombination on lasing in heterostructured quantum dots with engineered core/shell interfaces. *Nano Lett.* **15**, 7319−7328 (2015). https://doi.org/10.1021/acs.nanolett.5b02595.
66. Zavelani-Rossi, M. et al. Self-assembled CdSe/CdS nanorod micro-lasers fabricated from solution by capillary jet deposition. *Laser Photonics Rev.* **6**, 678−683 (2012). https://doi.org/10.1002/lpor.201200010.
67. Di Stasio, F. et al. Single-mode lasing from colloidal water-soluble CdSe/CdS quantum dot-in-rods. *Small* **11**, 1328−1334 (2015). https://doi.org/10.1002/smll.201402527.
68. Kelestemur, Y. et al. Alloyed heterostructures of $CdSe_xS_{1-x}$ nanoplatelets with highly tunable optical gain performance. *Chem. Mater.* **29**, 4857−4865 (2017). https://doi.org/10.1021/acs.chemmater.7b00829.
69. Moreels, I. et al. Nearly temperature-independent threshold for amplified spontaneous emission in colloidal CdSe/CdS quantum dot-in-rods. *Adv. Mater.* **24**, OP231−OP235 (2012). https://doi.org/10.1002/adma.201202067.
70. Biadala, L. et al. Tuning energy splitting and recombination dynamics of dark and bright excitons in CdSe/CdS dot-in-rod colloidal nanostructures. *J. Phys. Chem. C* **118**, 22309−22316 (2014). https://doi.org/10.1021/jp505887u.
71. Htoon, H., Hollingsworth, J. A., Dickerson, R. & Klimov, V. I. Effect of zero- to one-dimensional transformation on multiparticle auger recombination in semiconductor quantum rods. *Phys. Rev. Lett.* **91**, 227401 (2003). https://doi.org/10.1103/PhysRevLett.91.227401.
72. She, C., Demortiere, A., Shevchenko, E. V. & Pelton, M. Using shape to control photoluminescence from CdSe/CdS core/shell nanorods. *J. Phys. Chem. Lett.* **2**, 1469−1475 (2011). https://doi.org/10.1021/jz200510f.
73. Kazes, M., Oron, D., Shweky, I. & Banin, U. Temperature dependence of optical gain in CdSe/ZnS quantum rods. *J. Phys. Chem. C* **111**, 7898−7905 (2007). https://doi.org/10.1021/jp070075q.
74. Liu, H. et al. Spectral and nonlinear optical properties of quasi-type II CdSe/CdS nanotadpoles. *J. Phys. Chem. C* **124**, 27840−27847 (2020). https://doi.org/10.1021/acs.jpcc.0c09397.
75. Erdem, O. et al. Thickness-tunable self-assembled colloidal nanoplatelet films enable ultrathin optical gain media. *Nano Lett.* **20**, 6459−6465 (2020). https://doi.org/10.1021/acs.nanolett.0c02153.
76. Naeem, A. et al. Giant exciton oscillator strength and radiatively limited dephasing in two-dimensional platelets. *Phys. Rev. B* **91**, 121302(R) (2015). https://doi.org/10.1103/PhysRevB.91.121302.
77. Shornikova, E. V. et al. Negatively charged excitons in CdSe nanoplatelets. *Nano Lett.* **20**, 1370−1377 (2020). https://doi.org/10.1021/acs.nanolett.9b04907.
78. Bai, P. et al. CdSe/CdSeS nanoplatelet light-emitting diodes with ultrapure green color and high external quantum efficiency. *J. Phys. Chem. Lett.* **13**, 9051−9057 (2022). https://doi.org/10.1021/acs.jpclett.2c02633.
79. Zhang, J., Sun, Y., Ye, S., Song, J. & Qu, J. Heterostructures in two-dimensional CdSe nanoplatelets: synthesis, optical properties, and applications. *Chem. Mater.* **32**, 9490−9507 (2020). https://doi.org/10.1021/acs.chemmater.0c02593.
80. Liu, H. et al. Lateral surface passivation of CdSe nanoplatelets through crown management. *Nanoscale* **15**, 14140−14145 (2023). https://doi.org/10.1039/d3nr03133k.
81. Hu, A. et al. Green CdSe/CdSeS core/alloyed-crown nanoplatelets achieve unity photoluminescence quantum yield over a broad emission range. *Adv. Opt. Mater.* **10**, 2200469 (2022). https://doi.org/10.1002/adom.202200469.
82. Li, Q., Liu, Q., Schaller, R. D. & Lian, T. Reducing the optical gain threshold in two-dimensional CdSe nanoplatelets by the giant oscillator strength transition effect. *J. Phys. Chem. Lett.* **10**, 1624−1632 (2019). https://doi.org/10.1021/acs.jpclett.9b00759.
83. Li, Q. & Lian, T. Exciton spatial coherence and optical gain in colloidal two-dimensional cadmium chalcogenide nanoplatelets. *Acc. Chem. Res.* **52**, 2684−2693 (2019). https://doi.org/10.1021/acs.accounts.9b00252.
84. Wang, L., Dai, G., Deng, L. & Zhong, H. Progress in semiconductor quantum dots-based continuous-wave laser. *Sci. China Mater.* **63**, 1382−1397 (2020). https://doi.org/10.1007/s40843-020-1336-6.
85. Ivanov, S. A. et al. Light amplification using inverted core/shell nanocrystals: towards lasing in the single-exciton regime. *J. Phys. Chem. B* **108**, 10625−10630 (2004). https://doi.org/10.1021/jp0483371.
86. Klimov, V. I. et al. Single-exciton optical gain in semiconductor nanocrystals. *Nature* **447**, 441−446 (2007). https://doi.org/10.1038/nature05839.
87. Dang, C. et al. Red, green and blue lasing enabled by single-exciton gain in colloidal quantum dot films. *Nat. Nanotechnol.* **7**, 335−339 (2012). https://doi.org/10.1038/nnano.2012.61.
88. Kozlov, O. V. et al. Sub−single-exciton lasing using charged quantum dots coupled to a distributed feedback cavity. *Science* **365**, 672−675 (2019). https://doi.org/10.1126/science.aax3489.
89. Wu, K., Park, Y.-S., Lim, J. & Klimov, V. I. Towards zero-threshold optical gain using charged semiconductor quantum dots. *Nat. Nanotechnol.* **12**, 1140−1147 (2017). https://doi.org/10.1038/nnano.2017.189.

90. Wang, Y. et al. Stimulated emission and lasing from CdSe/CdS/ZnS core-multi-shell quantum dots by simultaneous three-photon absorption. *Adv. Mater.* **26**, 2954−2961 (2014). https://doi.org/10.1002/adma.201305125.
91. Li, J. et al. Enhanced performance of two-photon excited amplified spontaneous emission by cd-alloyed $CsPbBr_3$ nanocrystals. *Inorg. Chem.* **61**, 4735−4742 (2022). https://doi.org/10.1021/acs.inorgchem.2c00077.
92. Kenry, Z., Duan, Y. & Liu, B. Recent advances of optical imaging in the second near-infrared window. *Adv. Mater.* **30**, 1802394 (2018). https://doi.org/10.1002/adma.201802394.
93. Ren, C. et al. A near-infrared I emissive dye: toward the application of saturable absorber and multiphoton fluorescence microscopy in the deep-tissue imaging window. *Chem. Commun.* **55**, 5111−5114 (2019). https://doi.org/10.1039/c9cc02120e.
94. Zheng, Q. et al. Frequency-upconverted stimulated emission by simultaneous five-photon absorption. *Nat. Photonics* **7**, 234−239 (2013). https://doi.org/10.1038/nphoton.2012.344.
95. Chang, H. et al. Colloidal quantum dot lasers built on a passive two-dimensional photonic crystal backbone. *Nanoscale* **8**, 6571−6576 (2016). https://doi.org/10.1039/c5nr08544f.
96. Wang, Y. et al. Robust whispering-gallery-mode microbubble lasers from colloidal quantum dots. *Nano Lett.* **17**, 2640−2646 (2017). https://doi.org/10.1021/acs.nanolett.7b00447.
97. Wang, X., Yu, J. & Chen, R. Optical characteristics of ZnS passivated CdSe/CdS quantum dots for high photostability and lasing. *Sci. Rep.* **8**, 17323 (2018). https://doi.org/10.1038/s41598-018-35768-8.
98. Wang, Y. et al. Blue liquid lasers from solution of CdZnS/ZnS ternary alloy quantum dots with quasi-continuous pumping. *Adv. Mater.* **27**, 169−175 (2015). https://doi.org/10.1002/adma.201403237.
99. Signorini, R. et al. Facile production of up-converted quantum dot lasers. *Nanoscale* **3**, 4109−4113 (2011). https://doi.org/10.1039/c1nr10801h.
100. Gheshlaghi, N. et al. Self-resonant microlasers of colloidal quantum wells constructed by direct deep patterning. *Nano Lett.* **21**, 4598−4605 (2021). https://doi.org/10.1021/acs.nanolett.1c00464.
101. Lin, H.-T. et al. Boost lasing performances of 2D semiconductor in a hybrid tungsten diselenide monolayer/cadmium selenide quantum dots microcavity laser. *Adv. Opt. Mater.* **10**, 2200799 (2022). https://doi.org/10.1002/adom.202200799.
102. Yang, Z., Pelton, M., Fedin, I., Talapin, D. V. & Waks, E. A room temperature continuous-wave nanolaser using colloidal quantum wells. *Nat. Commun.* **8**, 143 (2017). https://doi.org/10.1038/s41467-017-00198-z.
103. He, T. et al. Thermally activated delayed fluorescence organic dots for two-photon fluorescence lifetime imaging. *Appl. Phys. Lett.* **112**, 211102 (2018). https://doi.org/10.1063/1.5034375.
104. He, T. et al. Comparison studies of excitonic properties and multiphoton absorption of near-infrared-I-emitting Cu-doped InP and InP/ZnSe nanocrystals. *Opt. Lett.* **45**, 1350−1353 (2020). https://doi.org/10.1364/OL.384876.
105. Min, B. et al. Ultralow threshold on-chip microcavity nanocrystal quantum dot lasers. *Appl. Phys. Lett.* **89**, 191124 (2006). https://doi.org/10.1063/1.2387966.
106. Xie, W. et al. On-chip integrated quantum-dot-silicon-nitride microdisk lasers. *Adv. Mater.* **29**, 1604866 (2017). https://doi.org/10.1002/adma.201604866.
107. Zhu, Y. et al. On-chip single-mode distributed feedback colloidal quantum dot laser under nanosecond pumping. *ACS Photonics* **4**, 2446−2452 (2017). https://doi.org/10.1021/acsphotonics.7b00644.
108. Liao, C. et al. Ultralow-threshold single-mode lasing from phase-pure CdSe/CdS core/shell quantum dots. *J. Phys. Chem. Lett.* **7**, 4968−4976 (2016). https://doi.org/10.1021/acs.jpclett.6b02465.
109. Rong, K., Sun, C., Shi, K., Gong, Q. & Chen, J. Room-temperature planar lasers based on water-dripping microplates of colloidal quantum dots. *ACS Photonics* **4**, 1776−1784 (2017). https://doi.org/10.1021/acsphotonics.7b00363.
110. Liu, H., Rong, K., Li, Z. & Chen, J. Experimental demonstration of nano-photonic devices and circuits with colloidal quantum dot waveguides. *Opt. Express* **28**, 23091−23104 (2020). https://doi.org/10.1364/OE.395088.
111. Jung, H. et al. Efficient on-chip integration of a colloidal quantum dot photonic crystal band-edge laser with a coplanar waveguide. *Opt. Express* **25**, 32919−32930 (2017). https://doi.org/10.1364/OE.25.032919.
112. Rong, K., Gan, F., Shi, K., Chu, S. & Chen, J. Configurable integration of on-chip quantum dot lasers and subwavelength plasmonic waveguides. *Adv. Mater.* **30**, 1706546 (2018). https://doi.org/10.1002/adma.201706546.
113. Kress, S. J. P. et al. A customizable class of colloidal-quantum-dot metallic lasers and amplifiers. *Sci. Adv.* **3**, e1700688 (2017). https://doi.org/10.1126/sciadv.1700688.
114. Rong, K., Liu, H., Shi, K. & Chen, J. Pattern-assisted stacking colloidal quantum dots for photonic integrated circuits. *Nanoscale* **11**, 13885−13893 (2019). https://doi.org/10.1039/c9nr01682a.
115. Diedenhofen, S. L., Kufer, D., Lasanta, T. & Konstantatos, G. Integrated colloidal quantum dot photodetectors with color-tunable plasmonic nanofocusing lenses. *Light: Sci. Appl.* **4**, e234 (2015). https://doi.org/10.1038/lsa.2015.7.
116. Zhu, B. et al. Integrated plasmonic infrared photodetector based on colloidal HgTe quantum dots. *Adv. Mater. Technol.* **4**, 1900354 (2019). https://doi.org/10.1002/admt.201900354.
117. Won, Y.-H. et al. Highly efficient and stable InP/ZnSe/ZnS quantum dot light-emitting diodes. *Nature* **575**, 634−638 (2019). https://doi.org/10.1038/s41586-019-1771-5.
118. Wei, H. et al. Blue lasing from heavy-metal-free colloidal quantum dots. *Laser Photonics Rev.* **17**, 2200557 (2023). https://doi.org/10.1002/lpor.202200557.
119. Chen, W. et al. Giant five-photon absorption from multidimensional core-shell halide perovskite colloidal nanocrystals. *Nat. Commun.* **8**, 15198 (2017). https://doi.org/10.1038/ncomms15198.
120. Zhu, B.-H., Zhang, H.-C., Zhang, Z.-Y., Cui, Y.-P. & Zhang, J.-Y. Effect of shell thickness on two-photon absorption and refraction of colloidal CdSe/CdS core/shell nanocrystals. *Appl. Phys. Lett.* **99**, 231903 (2011). https://doi.org/10.1063/1.3665400.
121. Zhu, B. H., Zhang, H. C., Zhang, J. Y., Cui, Y. P. & Zhou, Z. Q. Surface-related two-photon absorption and refraction of CdSe quantum dots. *Appl. Phys. Lett.* **99**, 021908 (2011). https://doi.org/10.1063/1.3610561.


## MISCELLANEA

**Acknowledgments** The authors acknowledge the assistance of SUSTech Core Research Facilities. This work is supported by the National Natural Science Foundation of China (62174079), Science, Technology and Innovation Commission of Shenzhen Municipality (Projects Nos. JCYJ20220530113015035, JCYJ20210324120204011, JCYJ20190808121211510, and KQTD2015071710313656).

**Declaration of competing interest** The authors declare no competing interests.